Journal of Contaminant Hydrology 181 (2015) 82–101

Contents lists available at ScienceDirect

Journal of Contaminant Hydrology

journal homepage: www.elsevier.com/locate/jconhyd

Modeling the co-transport of viruses and colloids in unsaturated porous media

N. Seetha [a], M.S. Mohan Kumar [a,b,*], S. Majid Hassanizadeh [c]

[a] Department of Civil Engineering, Indian Institute of Science, Bangalore, 560012, India
[b] Indo-French Cell for Water Sciences, Indian Institute of Science, Bangalore, 560012, India
[c] Department of Earth Sciences, Utrecht University, P.O. Box 80021, 3508 TA Utrecht, The Netherlands

ARTICLE INFO

Article history:
Received 17 July 2014
Received in revised form 14 January 2015
Accepted 20 January 2015
Available online 28 January 2015

Keywords:
Modeling
Co-transport
Virus
Colloid
Unsaturated porous medium

ABSTRACT

A mathematical model is developed to simulate the co-transport of viruses and colloids in unsaturated porous media under steady-state flow conditions. The virus attachment to the mobile and immobile colloids is described using a linear reversible kinetic model. Colloid transport is assumed to be decoupled from virus transport; that is, we assume that colloids are not affected by the presence of attached viruses on their surface. The governing equations are solved numerically using an alternating three-step operator splitting approach. The model is verified by fitting three sets of experimental data published in the literature: (1) Syngouna and Chrysikopoulos (2013) and (2) Walshe et al. (2010), both on the co-transport of viruses and clay colloids under saturated conditions, and (3) Syngouna and Chrysikopoulos (2015) for the co-transport of viruses and clay colloids under unsaturated conditions. We found a good agreement between observed and fitted breakthrough curves (BTCs) under both saturated and unsaturated conditions. Then, the developed model was used to simulate the co-transport of viruses and colloids in porous media under unsaturated conditions, with the aim of understanding the relative importance of various processes on the co-transport of viruses and colloids in unsaturated porous media. The virus retention in porous media in the presence of colloids is greater during unsaturated conditions as compared to the saturated conditions due to: (1) virus attachment to the air–water interface (AWI), and (2) co-deposition of colloids with attached viruses on its surface to the AWI. A sensitivity analysis of the model to various parameters showed that the virus attachment to AWI is the most sensitive parameter affecting the BTCs of both free viruses and total mobile viruses and has a significant effect on all parts of the BTC. The free and the total mobile viruses BTCs are mainly influenced by parameters describing virus attachment to the AWI, virus interaction with mobile and immobile colloids, virus attachment to solid–water interface (SWI), and colloid interaction with SWI and AWI. The virus BTC is relatively insensitive to parameters describing the maximum adsorption capacity of the AWI for colloids, inlet colloid concentration, virus detachment rate coefficient from the SWI, maximum adsorption capacity of the AWI for viruses and inlet virus concentration.

1. Introduction

Colloids are abundant in the subsurface in both organic and inorganic forms such as clays, humic substances, metal oxides and biocolloids. They get mobilized from the vadose zone through infiltration events, chemical perturbations, weathering, biological activities etc. Because of their large surface area to volume ratio, they have significant adsorption capacity for a variety of contaminants such as metal ions (Grolimund et al., 1996; Pang and Simunek, 2006; Pang et al., 2005; Roy and Dzombak, 1997), organic matter (Choi and Corapcioglu, 1997; Roy and Dzombak, 1997), pesticides (de Jonge et al., 1998), radionuclides (Bekhit et al., 2006; Chen et al., 2005; Saiers and Hornberger, 1996), bacteria

* Corresponding author at: Department of Civil Engineering, Indian Institute of Science, Bangalore-560012, India. Tel.: +91 80 2293 2814; fax: +91 80 2360 0404.
E-mail address: msmk@civil.iisc.ernet.in (M.S. Mohan Kumar).

http://dx.doi.org/10.1016/j.jconhyd.2015.01.002
0169-7722/

(Pang and Simunek, 2006; Vasiliadou and Chrysikopoulos, 2011; Yang et al., 2012), viruses (Jin et al., 2000; Syngouna and Chrysikopoulos, 2013, 2015; Walshe et al., 2010) and engineered nanoparticles (Cai et al., 2014). Colloids have been observed to act as carriers to transport contaminants. They have been found to either enhance (Cai et al., 2014; Chen et al., 2005; Flury and Qiu, 2008; Jin et al., 2000; Pang and Simunek, 2006; Saiers and Hornberger, 1996; Walshe et al., 2010) or retard (Flury and Qiu, 2008; Syngouna and Chrysikopoulos, 2013; Vasiliadou and Chrysikopoulos, 2011; Walshe et al., 2010; Yang et al., 2012) the movement of strongly adsorbing contaminants in porous media depending on the relative importance of the colloid and contaminant interactions with the porous medium, and contaminant interaction with colloids. Failure to account for the role of colloids in contaminant transport can lead to serious underestimation or overestimation of the travel distances of groundwater contaminants.

Groundwater gets contaminated with pathogenic bacteria, viruses, and protozoa from various sources such as septic tanks, leaking sewer lines, sanitary landfills, land application of wastewater and treatment plant sludge, and artificial recharge of groundwater. Viruses in groundwater are of major concern because of their small size, high infectivity and persistence (Hijnen et al., 2005; Schijven and Hassanizadeh, 2000; Yates et al., 1985). A number of factors such as the flow velocity (Hijnen et al., 2005; Keller et al., 2004; Syngouna and Chrysikopoulos, 2012), solution chemistry (Bales et al., 1991; Knappett et al., 2008; Loveland et al., 1996; Sadeghi et al., 2011, 2013; Zhuang and Jin, 2002; Zhuang and Jin, 2008), type of virus (Chu et al., 2001; Syngouna and Chrysikopoulos, 2012; Zhuang and Jin, 2002), temperature (Yates et al., 1985), grain size and shape (Knappett et al., 2008; Syngouna and Chrysikopoulos, 2012), soil surface characteristics (Chu et al., 2001; Zhuang and Jin, 2002), degree of water saturation (Anders and Chrysikopoulos, 2009; Chu et al., 2001; Torkzaban et al., 2006a,b), and presence of colloids (Jin et al, 2000; Syngouna and Chrysikopoulos, 2013, 2015; Walshe et al., 2010) have been found to affect virus transport in porous media. Syngouna and Chrysikopoulos (2013) and Walshe et al. (2010) conducted column experiments to study the co-transport of viruses and clay colloids under saturated conditions. They observed that colloids can either enhance or retard the transport of viruses depending on the relative importance of the interaction of the colloid and the virus with the porous medium and virus–colloid interactions. Also, virus retention in porous media increases in the presence of clay colloids because of the retention of some clay-bound viruses in the column due to colloid attachment to the grain surface (Syngouna and Chrysikopoulos, 2013, 2015; Walshe et al., 2010). Many researchers have studied the effect of the degree of water saturation on virus (and colloid) transport in porous media (Anders and Chrysikopoulos, 2009; Chu et al., 2001; Saiers and Lenhart, 2003; Torkzaban et al., 2006a,b; Wan and Wilson, 1994a). They observed that the virus (and colloid) retention in porous media increases as the degree of saturation decreases due to: (i) the attachment of the virus (and colloid) to the air–water interface (AWI) and (ii) the increased deposition at the solid–water interface (SWI) caused by the reduced diffusion length at low water contents. Similar results were found in colloid transport experiments in micromodels under two-phase flow, performed recently by Zhang et al. (2013a,b).

The effect of the presence of colloids on virus transport in saturated soil and the influence of the degree of water saturation on virus transport in unsaturated porous media have been widely studied separately from each other. Recently, Syngouna and Chrysikopoulos (2015) conducted column experiments to study the co-transport of viruses and clay colloids under unsaturated conditions. They observed that there is more virus retention in porous media in the presence of clay colloids during unsaturated conditions as compared to the saturated conditions.

Many researchers have developed mathematical models to simulate the colloid- or bacteria-associated transport of contaminants in porous media under saturated conditions (Corapcioglu and Jiang, 1993; Corapcioglu and Kim, 1995; Jiang and Corapcioglu, 1993; Kanti Sen et al., 2004; Kim and Corapcioglu, 1996; Saiers and Hornberger, 1996; van de Weerd and Leijnse, 1997) as well as variably saturated conditions (Choi and Corapcioglu, 1997; Massoudieh and Ginn, 2007; Simunek et al., 2006, 2012). Also, contaminant transport in porous media, in the presence of both bacteria and colloids, has been modeled by Bekhit et al. (2009), Kim and Corapcioglu (2002a,b) and Kim et al. (2003). The above models describe the transport of dissolved contaminants such as metal ions, organic matter, pesticides, radionuclides etc. in the presence of colloids or bacteria. One major difference between transport of dissolved contaminants and viruses under unsaturated conditions is that dissolved contaminants do not directly interact with the AWI under unsaturated conditions. But, viruses are themselves colloids and hence, they may have interactions with the SWI and AWI. Hence, the previously published colloid-facilitated contaminant transport models cannot be applied to simulate the co-transport of viruses and colloids under unsaturated conditions. Vasiliadou and Chrysikopoulos (2011) and recently, Katzourakis and Chrysikopoulos (2014) developed models to simulate the co-transport of bacteria and colloids, and viruses and colloids, in saturated porous media.

The objective of the current study is to develop a one-dimensional mathematical model to simulate the co-transport of viruses and colloids in partially saturated porous media under steady-state flow conditions. The developed model is used to simulate the results of three sets of experiments conducted by (a) Syngouna and Chrysikopoulos (2013) and (b) Walshe et al. (2010) for the co-transport of viruses and clay colloids under saturated conditions, and (3) Syngouna and Chrysikopoulos (2015) for the co-transport of viruses and clay colloids under unsaturated conditions. A sensitivity analysis of the model to various parameters under unsaturated conditions is performed so as to understand the relative importance of various processes on the co-transport of viruses and colloids in unsaturated porous media.

2. Mathematical model

In this section, we provide a mathematical model for the co-transport of viruses and colloids in porous media under unsaturated flow conditions. This is the first mathematical formulation of these processes for unsaturated conditions. A three-dimensional model for the co-transport of viruses and colloids under fully saturated conditions has been recently published by Katzourakis and Chrysikopoulos (2014).

Unsaturated porous medium can be idealized as having three phases: aqueous phase, solid phase and the air phase. Fig. 1 shows the schematic of the unsaturated porous medium indicating the different forms in which colloids and viruses can exist. Colloids can exist in three different forms: mobile colloids in aqueous phase, immobile colloids attached to SWI and immobile colloids attached to AWI, and viruses can exist in six different forms: free viruses in aqueous phase, attached to SWI, attached to AWI, attached to mobile colloids, and attached to immobile colloids at SWI and AWI. Various assumptions involved in this model are: (1) colloids do not affect the flow through the porous medium, (2) colloid transport is not affected by the presence of deposited viruses on its surface, and (3) virus inactivation is negligible. Fig. 2 shows the conceptual representation of various interactions among viruses, colloids, SWI and AWI in an unsaturated porous media. Both the colloid and virus deposition onto the SWI is assumed to be reversible whereas their deposition onto the AWI is assumed to be irreversible. The virus deposition onto the mobile as well as immobile colloids is assumed to be reversible.

2.1. Colloid transport

The governing equation for colloid transport in an unsaturated porous medium accounting for colloid deposition onto the SWI and AWI is given as:

$$\frac{\partial(\theta c_c)}{\partial t}+\rho_b\frac{\partial s_c}{\partial t}+\frac{\partial(A_{AWI}s_{ca})}{\partial t}=\frac{\partial}{\partial z}\left(D_L{}^c\theta\frac{\partial c_c}{\partial z}\right)-\frac{\partial(q_c c_c)}{\partial z} \quad (1)$$

where, c_c [ML^{-3}] is mass concentration of colloids in the aqueous phase (mass of colloids per unit volume of aqueous phase), s_c [MM^{-1}] is the colloid mass fraction adsorbed to SWI (mass of colloids per unit mass of soil), s_{ca} [ML^{-2}] is the colloid concentration adsorbed to AWI (mass of colloids per unit area of AWI), θ is the water content, ρ_b [ML^{-3}] is the bulk density of the porous medium, A_{AWI} [L^2 L^{-3}] is the specific area of the AWI, D_L^c [L^2T^{-1}] is the dispersion coefficient of colloids, $q_c=\theta v_c$ [LT^{-1}] is the Darcy flux of colloids, v_c [LT^{-1}] is the pore-water velocity of colloids, z [L] is the spatial coordinate and t [T] is the time.

Colloid deposition onto the SWI is assumed to be described by either a one-site linear reversible kinetic model (Corapcioglu and Choi, 1996; Noell et al., 1998; Vasiliadou and Chrysikopoulos, 2011) or a two-site kinetic model with site-1 being reversible and site-2 being irreversible (Compere et al., 2001; Yan, 1996). The corresponding mass balance equations for colloid adsorption to SWI with one-site (Eq. (2)) and two-site (Eq. (3a–c)) kinetic models are:

$$\rho_b\frac{\partial s_c}{\partial t}=k_{cs}\theta c_c-k_{sc}\rho_b s_c \quad (2)$$

$$\rho_b\frac{\partial s_{c1}}{\partial t}=k_{cs1}\theta c_c-k_{sc1}\rho_b s_{c1} \quad (3a)$$

$$\rho_b\frac{\partial s_{c2}}{\partial t}=k_{cs2}\theta c_c \quad (3b)$$

$$\frac{\partial s_c}{\partial t}=\frac{\partial s_{c1}}{\partial t}+\frac{\partial s_{c2}}{\partial t} \quad (3c)$$

where the subscripts 1 and 2 refer to sites 1 and 2, respectively, k_{cs} [T^{-1}] and k_{sc} [T^{-1}] are the colloid attachment and detachment rate coefficients for SWI, respectively.

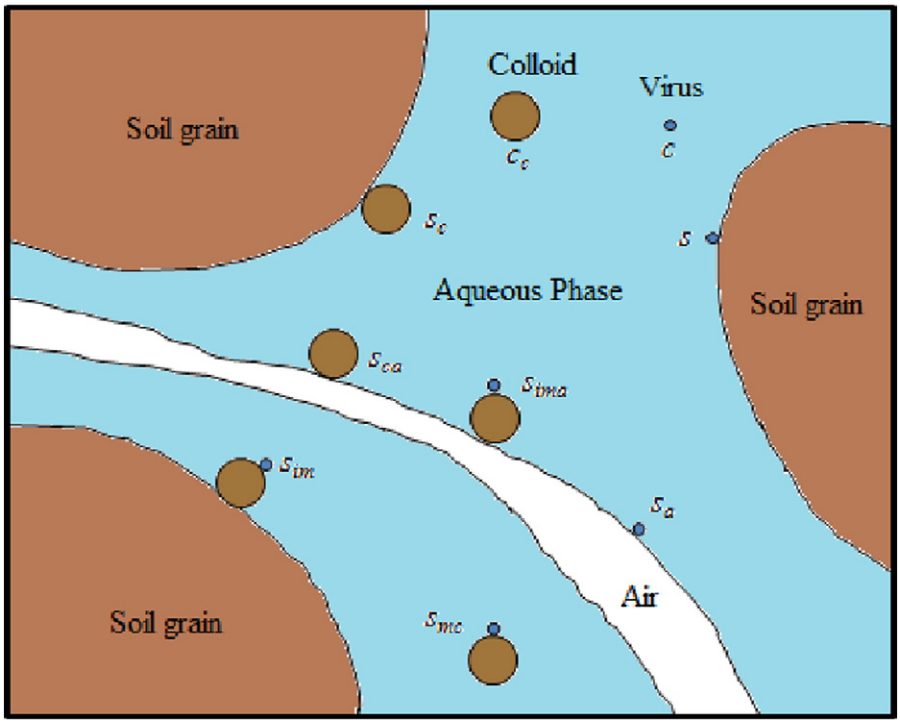

Fig. 1. Schematic representation of unsaturated porous medium with colloids and viruses.

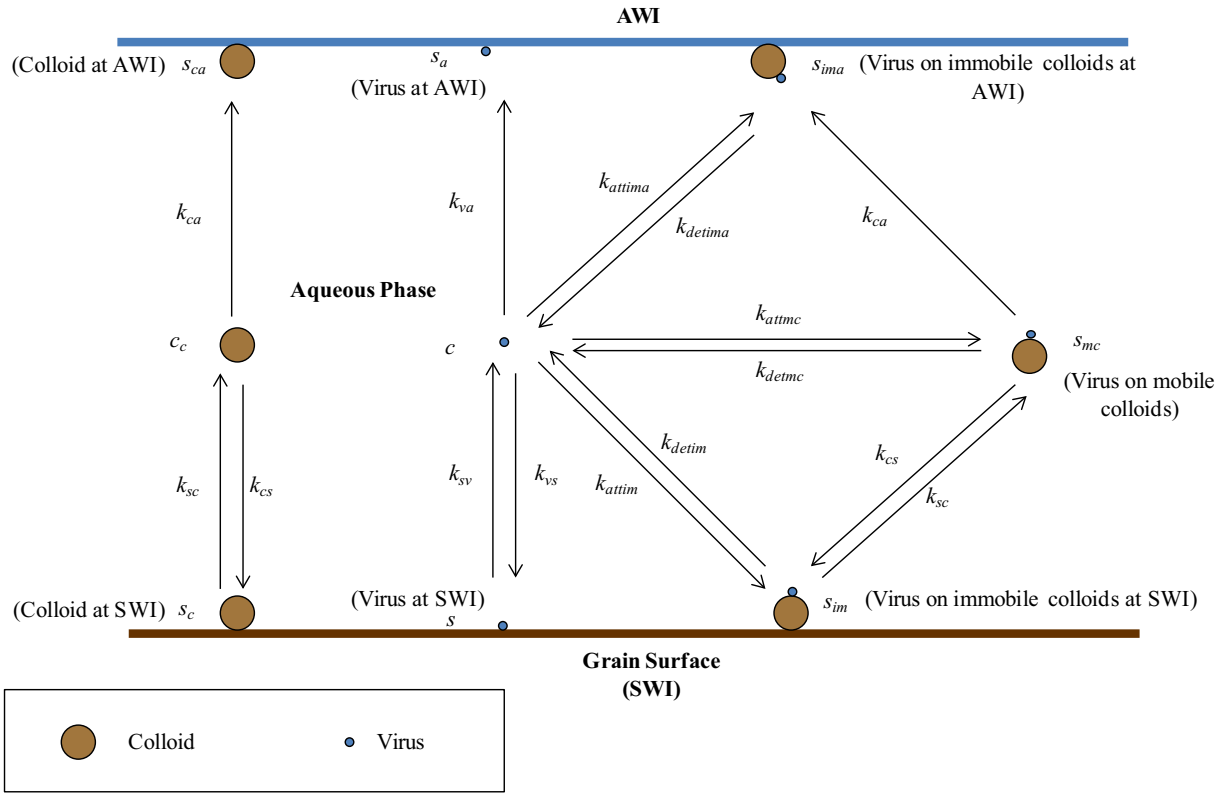

Fig. 2. Conceptual representation of various interactions in an unsaturated porous media. (Inspired from Fig. 1 of Simunek et al., 2006.)

Pore-scale visualization studies (Sirivithayapakorn and Keller, 2003; Wan and Wilson, 1994b) have observed that the colloids are retained irreversibly at the AWI by the capillary forces under steady-flow conditions. The mass balance equation for colloid deposition onto AWI, assuming a second-order irreversible kinetic model with blocking (Corapcioglu and Choi, 1996; Lenhart and Saiers, 2002; Saiers and Lenhart, 2003), is given as:

$$\frac{\partial(A_{AWI}s_{ca})}{\partial t} = k_{ca}\theta c_c \psi_c \tag{4}$$

where k_{ca} [T^{-1}] is the colloid attachment rate coefficient for AWI, $\psi_c = \frac{s_{ca(\max)} - s_{ca}}{s_{ca(\max)}}$ is the Langmuir blocking function representing the fraction of the AWI available for colloid deposition and $s_{ca(\max)}$ [ML^{-2}] is the maximum adsorption capacity of AWI for colloids. The specific AWI area, A_{AWI} is calculated using the formula derived by Cary (1994) (based on the capillary tube analogy) expressed in terms of the van Genuchten water retention function parameters as given in Niemet et al. (2002) (Kim et al., 2008):

$$A_{AWI} = \frac{\rho g n}{\sigma}\frac{m}{\alpha}B(w,z)[1 - I_u(w,z)] \tag{5}$$

$$u = \Theta^{1/m} \qquad \Theta = \frac{\theta - \theta_r}{\theta_s - \theta_r} \qquad w = m - \frac{1}{n} \qquad z = 1 + \frac{1}{n} \tag{6}$$

where ρ [ML^{-3}] is the density of water, g [LT^{-2}] is the gravitational constant, σ [MT^{-2}] is the surface tension of water, m [–], n [–] and α [L^{-1}] are the van Genuchten water retention function parameters, $B(w, z)$ represents the beta function of w and z, $I_u(w, z)$ is the incomplete beta function of w and z, Θ is the relative saturation, θ_s is the saturated water content and θ_r is the residual water content.

2.2. Virus transport

The governing equation for virus transport in an unsaturated porous medium accounting for virus deposition onto the SWI and AWI and virus attachment to mobile and immobile colloids is given as:

$$\frac{\partial(\theta c)}{\partial t} + \rho_b\frac{\partial s}{\partial t} + \frac{\partial(A_{AWI}s_a)}{\partial t} + \frac{\partial(\theta s_{mc}c_c)}{\partial t} + \rho_b\frac{\partial(s_{im}s_c)}{\partial t} + \frac{\partial(A_{AWI}s_{ima}s_{ca})}{\partial t} = \frac{\partial}{\partial z}\left(D_L\theta\frac{\partial c}{\partial z}\right) + \frac{\partial}{\partial z}\left(D_L{}^c\theta\frac{\partial(s_{mc}c_c)}{\partial z}\right) - \frac{\partial(qc)}{\partial z} - \frac{\partial(q_c s_{mc}c_c)}{\partial z} \tag{7}$$

where, c [pfu L^{-3}] is free virus concentration in the aqueous phase (number of viruses per unit volume of aqueous phase), s [pfu M^{-1}] is the virus concentration adsorbed to SWI (number of viruses per unit mass of dry soil), s_a [pfu L^{-2}] is the virus concentration adsorbed to AWI (number of viruses per unit area of AWI), s_{mc} [pfu M^{-1}], s_{im} [pfu M^{-1}] and s_{ima} [pfu M^{-1}] are the virus concentrations attached to mobile colloids, immobile colloids at SWI and immobile colloids at AWI, respectively (number of viruses per unit mass of mobile or immobile colloids), D_L [L^2T^{-1}] is the dispersion coefficient of viruses, $q = \theta v$ [LT^{-1}] is the Darcy flux and v [LT^{-1}] is the pore-water velocity.

Virus deposition onto the SWI is assumed to be described by a linear reversible kinetic model (Anders and Chrysikopoulos, 2009; Chu et al., 2001; Torkzaban et al., 2006a,b):

$$\rho_b \frac{\partial s}{\partial t} = k_{vs}\theta c - k_{sv}\rho_b s \tag{8}$$

where k_{vs} [T^{-1}] and k_{sv} [T^{-1}] are the virus attachment and detachment rate coefficients for SWI. The mass balance equation for virus attached to AWI, assuming a second-order irreversible kinetic model with blocking (Chu et al., 2001), is given as:

$$\frac{\partial (A_{AWI} s_a)}{\partial t} = k_{va}\theta c \psi_v \tag{9}$$

where k_{va} [T^{-1}] is the virus attachment rate coefficient for AWI, $\psi_v = \frac{s_{a(\max)} - s_a}{s_{a(\max)}}$ is the Langmuir blocking function for virus attachment to AWI, representing the fraction of the AWI available for virus deposition and $s_{a(\max)}$ [pfu L^{-2}] is the maximum adsorption capacity of AWI for viruses.

Virus interaction with mobile and immobile colloids is assumed to be described by a linear reversible kinetic model. The mass balance equations for viruses attached to the mobile colloids in case of one-site (Eq. (10)) and two-site (Eq. (11)) kinetic models for colloid interaction with the SWI can be written as:

$$\begin{aligned}\frac{\partial (\theta s_{mc} c_c)}{\partial t} = {} & \frac{\partial}{\partial z}\left(D_L{}^c \theta \frac{\partial (s_{mc} c_c)}{\partial z}\right) - \frac{\partial (q_c s_{mc} c_c)}{\partial z} \\ & + k_{attmc}\theta c - k_{detmc}\theta s_{mc} c_c - k_{cs}\theta s_{mc} c_c \\ & + k_{sc}\rho_b s_c s_{im} - k_{ca}\theta s_{mc} c_c \psi_c\end{aligned} \tag{10}$$

$$\begin{aligned}\frac{\partial (\theta s_{mc} c_c)}{\partial t} = {} & \frac{\partial}{\partial z}\left(D_L{}^c \theta \frac{\partial (s_{mc} c_c)}{\partial z}\right) - \frac{\partial (q_c s_{mc} c_c)}{\partial z} + k_{attmc}\theta c \\ & - k_{detmc}\theta s_{mc} c_c - k_{cs1}\theta s_{mc} c_c + k_{sc1}\rho_b s_{c1} s_{im1} \\ & - k_{cs2}\theta s_{mc} c_c - k_{ca}\theta s_{mc} c_c \psi_c\end{aligned} \tag{11}$$

where k_{attmc} [T^{-1}] and k_{detmc} [T^{-1}] are the virus attachment and detachment rate coefficients for the mobile colloids. The mass balance equation for viruses attached to immobile colloids at SWI corresponding to one-site (Eq. (12)) and two-site (Eq. (13a–b)) kinetic models for colloid interaction with the SWI is given as:

$$\begin{aligned}\rho_b \frac{\partial (s_{im1} s_{c1})}{\partial t} = {} & k_{attim}\theta c - k_{detim}\rho_b s_{im1} s_{c1} \\ & + k_{cs1}\theta s_{mc} c_c - k_{sc1}\rho_b s_{im1} s_{c1}\end{aligned} \tag{12}$$

$$\begin{aligned}\rho_b \frac{\partial (s_{im1} s_{c1})}{\partial t} = {} & k_{attim}\theta c - k_{detim}\rho_b s_{im1} s_{c1} \\ & + k_{cs1}\theta s_{mc} c_c - k_{sc1}\rho_b s_{im1} s_{c1}\end{aligned} \tag{13a}$$

$$\rho_b \frac{\partial (s_{im2} s_{c2})}{\partial t} = k_{attim}\theta c - k_{detim}\rho_b s_{im2} s_{c2} + k_{cs2}\theta s_{mc} c_c \tag{13b}$$

$$\frac{\partial (s_{im} s_c)}{\partial t} = \frac{\partial (s_{im1} s_{c1})}{\partial t} + \frac{\partial (s_{im2} s_{c2})}{\partial t} \tag{13c}$$

where k_{attim} [T^{-1}] and k_{detim} [T^{-1}] are the virus attachment and detachment rate coefficients for immobile colloids at SWI. The mass balance equation for viruses attached to the immobile colloids at the AWI is given as:

$$\frac{\partial (A_{AWI} s_{ima} s_{ca})}{\partial t} = k_{attima}\theta c - k_{detima} A_{AWI} s_{ima} s_{ca} + k_{ca}\theta \psi_c s_{mc} c_c \tag{14}$$

where k_{attima} [T^{-1}] and k_{detima} [T^{-1}] are the virus attachment and detachment rate coefficients for immobile colloids at AWI.

3. Solution of the governing equations

Eqs. (1)–(4) and (7)–(14) constitute the complete set of coupled equations governing the co-transport of colloids and viruses in an unsaturated porous medium. They comprise nine equations for nine variables (c_c, s_c, s_{ca}, c, s, s_a, s_{mc}, s_{im} and s_{ima}) in case of a one-site kinetic model for SWI colloid attachment and eleven equations in terms of eleven variables (c_c, s_{c1}, s_{c2}, s_{ca}, c, s, s_a, s_{mc}, s_{im1}, s_{im2} and s_{ima}) in case of a two-site kinetic model for SWI colloid attachment. The complete set of governing Eqs. (1)–(4) and (7)–(14) are solved subject to the following initial and boundary conditions:

$$c_c(z,0) = s_c(z,0) = s_{ca}(z,0) = 0 \tag{15}$$

$$c(z,0) = s(z,0) = s_a(z,0) = s_{mc}(z,0) = s_{im}(z,0) = s_{ima}(z,0) = 0 \tag{16}$$

$$c_c(0,t) = \begin{cases} c_{c0} & t \le t_{in} \\ 0 & t > t_{in} \end{cases} \tag{17}$$

$$c(0,t) = \begin{cases} c_0 & t \le t_{in} \\ 0 & t > t_{in} \end{cases} \tag{18}$$

$$s_{mc} c_c(0,t) = 0 \tag{19}$$

$$\frac{\partial c_c}{\partial z}(L,t) = 0 \tag{20}$$

$$\frac{\partial c}{\partial z}(L,t) = 0 \tag{21}$$

$$\frac{\partial s_{mc} c_c}{\partial z}(L,t) = 0 \tag{22}$$

where c_{c0} and c_0 are the inlet colloid and free virus concentrations, respectively, t_{in} is the duration of the input pulse and L is the length of the column. Eqs. (15) and (16), respectively, indicate that there is no colloid and virus concentrations present inside the column initially. Eqs. (17) and (18), respectively, are the Dirichlet boundary conditions for colloid and virus concentrations at the inlet of the column. Eq. (19) implies that there are no viruses attached onto the mobile colloids entering at the inlet. Eqs. (20), (21) and (22) represent the Neumann type boundary conditions for aqueous phase colloids, free viruses, and viruses attached to mobile colloids, respectively, at the column outlet.

As colloid transport is assumed to be not affected by the presence of attached viruses on its surface, equations governing colloid transport are solved first at every time step and then virus transport equations are solved. The governing equations are solved numerically using an alternating three-step operator splitting approach (Barry et al., 2000; Gasda et al., 2011; Kaluaracbchi and Morshed, 1995) which allows splitting the coupled set of governing equations into advection, dispersion, and reaction operators which are then solved sequentially over the first half of each time step with the order of the solution of the advection, dispersion and reaction operators switched in the second half of the time step. The solution from one operator forms the initial condition for the following operator. Operator splitting method offers the flexibility of choosing the numerical scheme best suited for the solution of each operator. In this study, we use an explicit finite volume method based on Monotone Upwind Schemes for Conservation Laws to solve advective part which is globally second-order accurate and non-oscillatory (Putti et al., 1990; Ratha et al., 2009; Soraganvi and Mohan Kumar, 2009). We use a second-order Godunov-type scheme with a minmod limiter for the piecewise linear interpolation of concentration in each cell for calculating the advective flux at the cell interfaces, and Hancock's scheme for time splitting which is a two-step second-order accurate explicit scheme (Putti et al., 1990; Ratha et al., 2009; Soraganvi and Mohan Kumar, 2009). The stability of the above scheme depends on Courant number, $c_u = \frac{v\Delta t}{\Delta z}$, which should be less than or equal to one. The dispersive part is solved using a fully implicit finite difference method, and the reaction part using a fourth-order Runge–Kutta method. The uncoupled equations corresponding to colloid transport for one-site kinetic model for colloid attachment to the SWI and the sequence of solving them during the first half of each time step are:

$$\text{Advective transport}: \frac{\partial(\theta c_c)}{\partial t} = -\frac{\partial(q_c c_c)}{\partial z} \tag{23}$$

$$\text{Dispersive transport}: \frac{\partial(\theta c_c)}{\partial t} = \frac{\partial}{\partial z}\left(D_L{}^c \theta \frac{\partial c_c}{\partial z}\right) \tag{24}$$

$$\text{Reaction}: \begin{cases} \dfrac{d(\theta c_c)}{dt} = -k_{cs}\theta c_c + k_{sc}\rho_b s_c - k_{ca}\theta c_c \psi_c \\ \rho_b \dfrac{ds_c}{dt} = k_{cs}\theta c_c - k_{sc}\rho_b s_c \\ \dfrac{d(A_{AWI} s_{ca})}{dt} = k_{ca}\theta c_c \psi_c \end{cases} \tag{25}$$

The order of solving the splitted Eqs. (23)–(25) is reversed during the second half of each time step. Following the solution of colloid transport, virus transport equations are solved at every time step. Similarly the splitted equations corresponding to virus transport and the sequence of solving them during the first half of each time step are:

$$\text{Advective transport for viruses attached to mobile colloids}: \frac{\partial(\theta s_{mc} c_c)}{\partial t} = -\frac{\partial(q_c s_{mc} c_c)}{\partial z} \tag{26}$$

$$\text{Dispersive transport for viruses attached to mobile colloids}: \frac{\partial(\theta s_{mc} c_c)}{\partial t} = \frac{\partial}{\partial z}\left(D_L{}^c \theta \frac{\partial(s_{mc} c_c)}{\partial z}\right) \tag{27}$$

$$\text{Advective transport for free viruses in aqueous phase}: \frac{\partial(\theta c)}{\partial t} = -\frac{\partial(qc)}{\partial z} \tag{28}$$

$$\text{Dispersive transport for free viruses in aqueous phase}: \frac{\partial(\theta c)}{\partial t} = \frac{\partial}{\partial z}\left(D_L \theta \frac{\partial c}{\partial z}\right) \tag{29}$$

$$\text{Reaction}: \begin{cases} \dfrac{d(\theta c)}{dt} = -k_{vs}\theta c + k_{sv}\rho s - k_{va}\theta c \psi_v - k_{attmc}\theta c + k_{detmc}\theta s_{mc} c_c - k_{attim}\theta c + k_{detim}\rho_b s_{im} s_c - k_{attima}\theta c + k_{detima} A_{AWI} s_{ima} s_{ca} \\ \rho_b \dfrac{ds}{dt} = k_{vs}\theta c - k_{sv}\rho_b s \\ \dfrac{d(A_{AWI} s_a)}{dt} = k_{va}\theta c \psi_v \\ \dfrac{d(\theta s_{mc} c_c)}{dt} = k_{attmc}\theta c - k_{detmc}\theta s_{mc} c_c - k_{cs}\theta s_{mc} c_c + k_{sc}\rho_b s_c s_{im} - k_{ca}\theta s_{mc} c_c \psi_c \\ \rho_b \dfrac{d(s_{im} s_c)}{dt} = k_{attim}\theta c - k_{detim}\rho_b s_{im} s_c + k_{cs}\theta s_{mc} c_c - k_{sc}\rho_b s_{im} s_c \\ \dfrac{d(A_{AWI} s_{ima} s_{ca})}{dt} = k_{attima}\theta c - k_{detima} A_{AWI} s_{ima} s_{ca} + k_{ca}\theta \psi_c s_{mc} c_c. \end{cases} \tag{30}$$

The order of solving the splitted Eqs. (26)–(30) is reversed during the second half of each time step.

4. Model verification

The model developed is verified using the column experimental data of (1) Syngouna and Chrysikopoulos (2013) and (2) Walshe et al. (2010) who studied the co-transport of viruses and clay colloids in porous media under saturated conditions, and (3) Syngouna and Chrysikopoulos (2015) for the co-transport of viruses and clay colloids in partially saturated porous media. The model verification also provided us the range of values of the parameters describing virus attachment and detachment rate coefficients with the colloids (k_{attmc}, k_{attim}, k_{attima}, k_{detmc}, k_{detim}, k_{detima}) to be used for unsaturated virus transport simulations.

4.1. Simulation of experiments of Syngouna and Chrysikopoulos (2013)

Syngouna and Chrysikopoulos (2013) studied the co-transport of bacteriophages, MS2 or ΦX174 with kaolinite or montmorillonite under saturated conditions in a 30-cm long column with 2.5 cm diameter, packed with 2-mm diameter glass beads. The packed column had a bulk density of 1.61 g cm^{-3} and a porosity of 0.42. The column was placed horizontally to minimize the gravity effects. All experiments were performed with sterile distilled deionized water (ddH_2O) (pH = 7, ionic strength = 0.0001 M). A fresh column was packed for each experiment. One set of experiments was performed with viruses and clay colloids separately in order to determine their individual transport characteristics. Another set of co-transport experiments was performed to investigate the effect of the presence of clay colloids on virus transport. Four sets of co-transport experiments were performed: ΦX174-kaolinite, ΦX174-montmorillonite, MS2-kaolinite and MS2-montmorillonite. For each experiment, the clay colloidal suspension and the viral suspension were injected simultaneously into the packed column at the same flow rate for 3 pore volumes (PVs), followed by 3 PVs of ddH_2O. All experiments were performed at three different flow rates of 2.5, 1.5 and 0.8 mL min^{-1}, corresponding to pore water velocities of 1.21, 0.74 and 0.38 cm min^{-1}, respectively. All experiments were carried out at room temperature (25 °C). Chloride, in the form of KCl, was chosen as the conservative tracer for the transport experiments. Detailed information about the experiments is available in Syngouna and Chrysikopoulos (2013).

We assumed a two-site linear kinetic model for clay colloid attachment to the solid grains, with a reversible and an irreversible site. Hence, our model with the set of Eqs. (1) and (3a–c) for colloid transport, and Eqs. (7), (8), (11) and (13a–c) for virus transport are used to fit the observed breakthrough curves from the co-transport of colloids and viruses under saturated conditions with the initial and boundary conditions specified by Eqs. (15)–(22).

The steps followed for fitting the observed BTCs from the co-transport experiments of Syngouna and Chrysikopoulos (2013) are briefly described here. For any flow rate, first the pore-water velocity and the dispersion coefficient values were estimated by fitting the tracer breakthrough curve. Colloids and viruses were assumed to travel at the same velocity and have the same dispersion coefficient as the tracer during both individual and co-transport experiments. Next, the virus and colloid BTCs from the individual transport experiments were fitted with our model so as to estimate the virus and colloid deposition parameters for the solid surface (k_{vs} & k_{sv} and k_{cs1}, k_{sc1} & k_{cs2}), respectively. The colloid deposition parameters for the solid surface (k_{cs1}, k_{sc1} *and* k_{cs2}) were also estimated from the colloid BTC of the co-transport experiments. This allowed us to determine the effect of the presence of viruses on colloid deposition behavior. The parameters estimated by fitting the BTC of viruses from the individual transport experiment (k_{vs} and k_{sv}) and colloids from the co-transport experiment (k_{cs1}, k_{sc1} *and* k_{cs2}) were used as input while fitting the free virus BTC from co-transport experiments. The free virus BTC during the co-transport experiments was fitted so as to estimate the virus attachment and detachment rate coefficients for the mobile and immobile colloids (k_{attmc}, k_{attim}, k_{detmc}, k_{detim}), assuming that the rate coefficients for virus interaction with the mobile and immobile colloids are the same ($k_{attmc} = k_{attim}$, $k_{detmc} = k_{detim}$). The parameters were estimated using Levenberg–Marquardt algorithm. Finally, knowing all parameter values, we used our model to obtain the total mobile virus BTC during the co-transport experiments and compared our results to the experimental data. The total mobile virus concentration is the sum of the free virus concentration and the virus concentration attached to the mobile colloids ($c + s_{mc}c_c$).

Though we fitted the breakthrough curves of all co-transport experiments at three different flow rates, here we show the verification for the flow rate of 0.8 mL min^{-1} only. Fig. 3 shows the observed and fitted BTCs of MS2, ΦX174, kaolinite and montmorillonite during the individual transport experiments at $Q = 0.8$ mL min^{-1}. It can be seen that the model fits the observed BTCs reasonably well. Fig. 4 shows the observed and fitted BTCs of colloids and viruses during the co-transport of ΦX174-kaolinite, ΦX174-montmorillonite, MS2-kaolinite and MS2-montmorillonite at $Q = 0.8$ mL min^{-1}. The fitted values of parameters at three different flow rates are given in Table 1. It can be seen from Fig. 4 that the model results are in good agreement with the observed data of colloids, free viruses and total mobile viruses for all co-transport experiments. Comparison of Figs. 3c, 4a and e show that the behavior of kaolinite colloids in soil is significantly affected by the presence of the viruses. Similar results are obtained for montmorillonite (compare Figs. 3d, 4c and g). In all cases, values of rate coefficients for colloid attachment to glass beads are larger during co-transport experiments compared to the transport of colloids alone. One hypothesis is that viruses attached to glass beads reduce the negative charge of their surfaces. The zeta potentials of MS2 and ΦX174 (MS2: -40.4 ± 3.7 mV, ΦX174: -31.78 ± 1.25 mV) are less negatively charged than the glass beads (-54.6 ± 2.4 mV) at the chemical conditions used in Syngouna and Chrysikopoulos (2013). Hence, the viruses deposited onto the glass beads enhance the favorability of colloid deposition onto the glass beads. This justification is supported by experimental results of Yang et al. (2012) who observed from column experiments that the bacteria retention in quartz sand increased in the presence of bentonite. Also, they observed that the bacteria retention was more in the case of sand with attached bentonite present on its surface initially but with no bentonite in suspension as compared to the case when the bentonite was present in the suspension but with no attached bentonite present on the sand initially. The increased bacterial retention in the case of sand with attached bentonite present on its

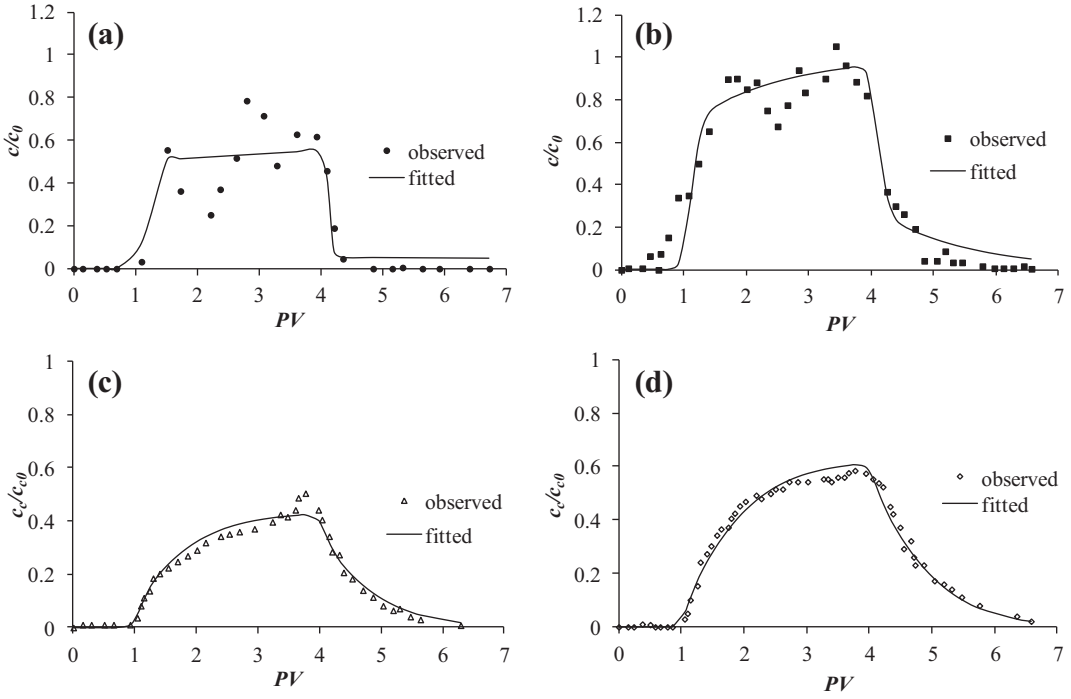

Fig. 3. Observed and fitted BTCs from Syngouna and Chrysikopoulos (2013) for (a) MS2, (b) ΦX174, (c) kaolinite and (d) montmorillonite during individual transport experiments at $Q = 0.8$ mL min^{-1}.

surface initially but with no bentonite in suspension might be because of the enhanced attachment of bacteria to bentonite already adsorbed to sand. As bentonite was found to be less negatively charged than the sand under the chemical conditions used by Yang et al. (2012), the bentonite attached to sand decreased the surface charge of sand making it less negative and thus increasing the bacterial deposition onto sand. They measured the zeta potential of the bacteria with and without bentonite particles in suspension and found that both are comparable, which indicated that the presence of bentonite did not have obvious influence on the electrokinetic properties of bacteria. The zeta potential of sand with attached bentonite was less negative than without attached bentonite, indicating that the attachment of bentonite onto quartz sand decreased the surface charge of quartz sand. From Figs. 3 and 4, it can be seen that both the MS2 and ΦX174 retention increases in the presence of clay colloids due to (i) the attachment of viruses to mobile and immobile colloids and (ii) increased attachment of clay colloids to grain surface in the presence of viruses. Recently, Katzourakis and Chrysikopoulos (2014) tested the accuracy of their three dimensional model for the co-transport of colloids and viruses in water saturated porous media by fitting the experimental data of Syngouna and Chrysikopoulos (2013). The model of Katzourakis and Chrysikopoulos (2014) differs from our model due to the following reasons: (1) Virus attachment to the irreversibly deposited colloids was neglected in Katzourakis and Chrysikopoulos (2014) whereas our model accounts for that; (2) Katzourakis and Chrysikopoulos (2014) included virus inactivation terms in their model whereas we have not considered the virus inactivation in the model as the duration of the experiments modeled in this study (Syngouna and Chrysikopoulos, 2013, 2015; Walshe et al., 2010) are very small; and (3) In Katzourakis and Chrysikopoulos (2014), virus attachment to the mobile and immobile colloids is limited by the colloid concentration in the mobile and immobile phases. As colloid concentration is usually much larger than the virus concentration (Syngouna and Chrysikopoulos, 2013, 2015; Walshe et al., 2010), we assumed in this paper also that virus attachment to colloids is not limited by the colloid concentration. Because of the above differences in the two models, the estimated parameter values are also different between our model and that of Katzourakis and Chrysikopoulos (2014).

4.2. Simulation of experiments of Walshe et al. (2010)

Walshe et al. (2010) studied the co-transport of kaolinite and bacteriophage MS2 in a 2-m long column with an internal diameter of 19 cm, packed with heterogeneous gravel aquifer materials under saturated conditions. The packed column had an effective porosity of 0.26, a bulk density of 1.91 g cm^{-3} and a pore volume of 15 L. Tapwater, which is untreated groundwater sourced from deep alluvial gravel aquifers, was used as the background electrolyte. A series of column experiments were conducted to investigate virus transport in the absence and presence of kaolinite as well as the impact of pH, ionic strength, dissolved organic matter, and flow rate on the co-transport of viruses and kaolinite. All experiments were carried out at a temperature of about 18 °C. The base case experiment was carried out to study virus transport with and without kaolinite colloids in unmodified tapwater (pH 7.5, ionic strength 1.65 mM, and dissolved organic matter < 0.1 mg L^{-1}) at a flow rate of 104 mL min^{-1}. For the co-transport experiments, the solution containing kaolinite and MS2 was mixed overnight in the dark to ensure the maximum attachment of MS2 phage

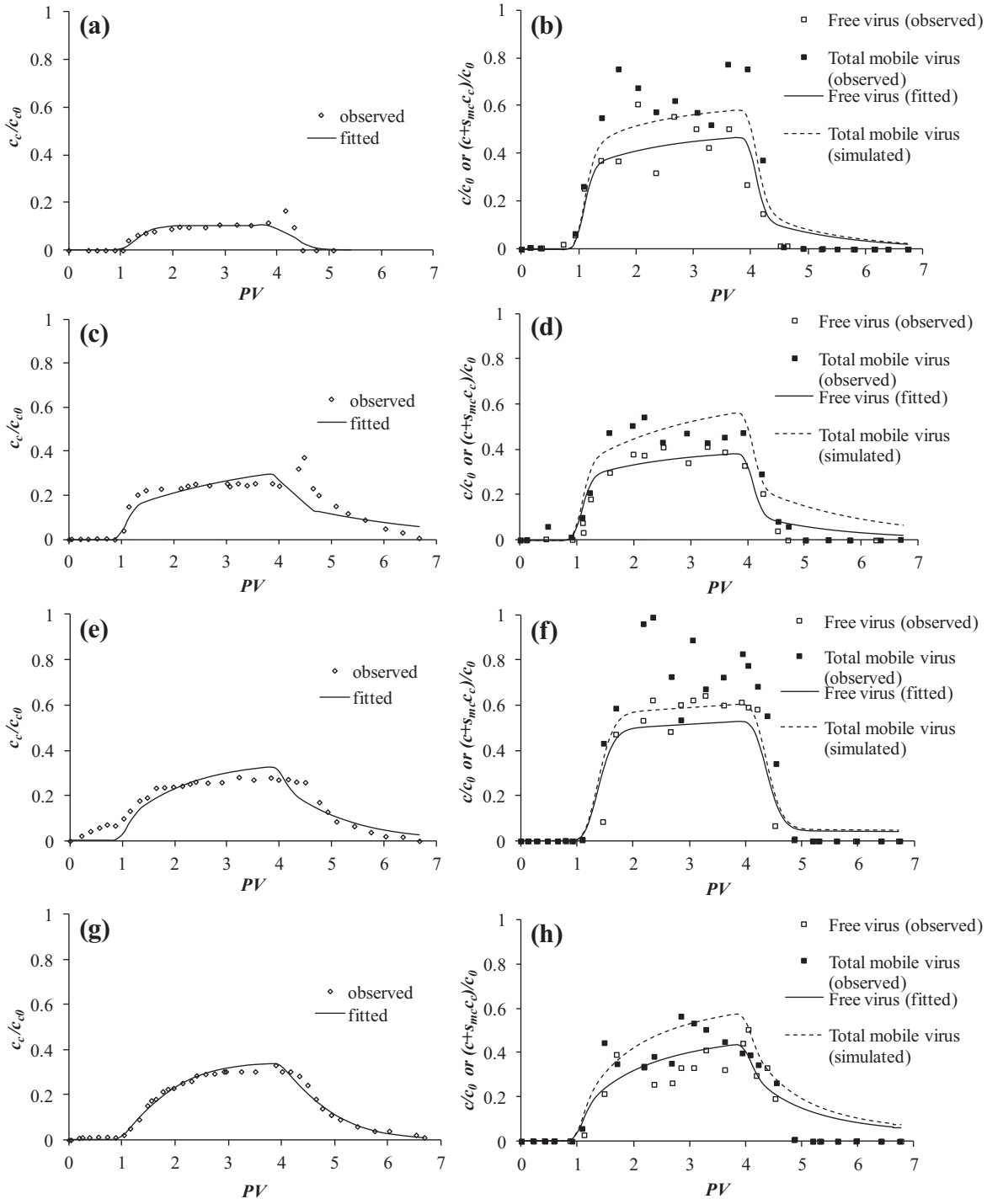

Fig. 4. Observed and fitted BTCs of colloids (left column) and viruses (right column) during co-transport experiments from Syngouna and Chrysikopoulos (2013) for (a, b) ΦX174-kaolinite, (c, d) ΦX174-montmorillonite, (e, f) MS2-kaolinite, and (g, h) MS2-montmorillonite at $Q = 0.8$ mL min^{-1}. (Free virus (fitted): The observed free virus BTC from the experiments is fitted with our model, Total mobile virus (simulated): Total mobile virus BTC is predicted using the parameter values estimated by fitting the free virus BTC).

to kaolinite prior to the injection of the solution into the column. The injection solutions contained approximately 300 mg L^{-1} kaolinite and MS2 phage with a total concentration of 1000 pfu mL^{-1} (free MS2 + MS2 attached to colloids in the influent). After the injection of one PV of the colloid–virus solution, the column was flushed with tapwater for two PVs, which did not contain any colloids or viruses. Between experiments the column was thoroughly flushed with normal

Table 1
Fitted values of model parameters for the experimental data of Syngouna and Chrysikopoulos (2013)[a].

Q (mL min^{-1})	Experiment	Individual transport							Co-transport						
		Virus[b]			Colloid[c]				Colloid[d]				Virus[e]		
		k_{vs} (min^{-1})	k_{sv} (min^{-1})	R^2	k_{cs1} (min^{-1})	k_{sc1} (min^{-1})	k_{cs2} (min^{-1})	R^2	k_{cs1} (min^{-1})	k_{sc1} (min^{-1})	k_{cs2} (min^{-1})	R^2	k_{attmc} (min^{-1})	k_{detmc} (min^{-1})	R^2 (free virus)
0.8	ΦX174-kaolinite	0.0041 (0.0008)	0.01 (0.003)	0.94	0.015 (0.001)	0.0294 (0.003)	0.0096 (0.0002)	0.97	0.045 (0.04)	0.187 (0.1)	0.026 (0.0005)	0.92	0.0027 (0.0002)	~0	0.87
	ΦX174-montmorillonite	0.0041 (0.0008)	0.01 (0.003)	0.94	0.0194 (0.001)	0.0322 (0.002)	0.0055 (0.0001)	0.98	0.011 (0.001)	0.0085 (0.003)	0.011 (0.001)	0.89	0.0036 (0.0002)	~0	0.92
	MS2-kaolinite	0.0079 (0.0008)	0.0007 (0.0004)	0.86	0.015 (0.001)	0.0294 (0.003)	0.0096 (0.0002)	0.97	0.014 (0.002)	0.02 (0.006)	0.012 (0.0006)	0.84	0.055 (0.02)	0.37 (0.05)	0.92
	MS2-montmorillonite	0.0079 (0.0008)	0.0007 (0.0004)	0.86	0.0194 (0.001)	0.0322 (0.002)	0.0055 (0.0001)	0.98	0.024 (0.002)	0.038 (0.004)	0.0123 (0.0001)	0.98	0.005 (0.002)	0.014 (0.005)	0.82
1.5	ΦX174-kaolinite	0.0049 (0.002)	0.02 (0.016)	0.82	0.022 (0.001)	0.052 (0.004)	0.012 (0.0002)	0.98	0.03 (0.004)	0.063 (0.01)	0.025 (0.0006)	0.97	0.011 (0.002)	0.0015 (0.0016)	0.54
	ΦX174-montmorillonite	0.0049 (0.002)	0.02 (0.016)	0.82	0.015 (0.0009)	0.036 (0.004)	0.0098 (0.0003)	0.98	0.144 (0.036)	0.14 (0.036)	0.032 (0.0007)	0.92	0.0069 (0.001)	0.0006 (0.001)	0.65
	MS2-kaolinite	0.0088 (0.001)	0.00055 (0.001)	0.86	0.022 (0.001)	0.052 (0.004)	0.012 (0.0002)	0.98	0.003 (0.002)	0.0086 (0.01)	0.012 (0.002)	0.96	0.014 (0.001)	~0	0.36
	MS2-montmorillonite	0.0088 (0.001)	0.00055 (0.001)	0.86	0.015 (0.0009)	0.036 (0.004)	0.0098 (0.0003)	0.98	0.006 (0.001)	0.02 (0.01)	0.015 (0.001)	0.97	0.01 (0.0009)	0.0014 (0.0009)	0.76
2.5	ΦX174-kaolinite	0.0085 (0.027)	0.035 (0.056)	0.22	0.0016 (0.018)	0.0057 (0.09)	0.0034 (0.018)	0.98	0.008 (0.005)	0.046 (0.08)	0.047 (0.003)	0.89	0.012 (0.0008)	~0	0.8
	ΦX174-montmorillonite	0.0085 (0.027)	0.035 (0.056)	0.22	0.018 (0.003)	0.054 (0.02)	0.016 (0.001)	0.94	0.017 (0.004)	0.11 (0.04)	0.03 (0.0007)	0.98	0.01 (0.0005)	~0	0.93
	MS2-kaolinite	0.044 (0.019)	0.146 (0.05)	0.95	0.0016 (0.018)	0.0057 (0.09)	0.0034 (0.018)	0.98	0.008 (0.0008)	0.026 (0.01)	0.021 (0.001)	0.99	0.032 (0.003)	0.0003 (0.001)	0.43
	MS2-montmorillonite	0.044 (0.019)	0.146 (0.05)	0.95	0.018 (0.003)	0.054 (0.02)	0.016 (0.001)	0.94	0.01 (0.004)	0.092 (0.04)	0.037 (0.0005)	0.99	0.018 (0.001)	~0	0.73

[a] The standard errors associated with the estimated parameter values are given in parentheses.
[b] k_{vs} and k_{sv} obtained by fitting the virus BTC from individual transport experiments.
[c] k_{cs1}, k_{sc1} and k_{cs2} obtained by fitting the colloid BTC from individual transport experiments.
[d] k_{cs1}, k_{sc1} and k_{cs2} obtained by fitting the colloid BTC from co-transport experiments.
[e] k_{attmc} and k_{detmc} obtained by fitting the free virus BTC from the co-transport experiments assuming $k_{attmc} = k_{attim}$ and $k_{detmc} = k_{detim}$. The values of k_{cs1}, k_{sc1} and k_{cs2} obtained by fitting the colloid BTC from co-transport experiments and, k_{vs} and k_{sv} obtained by fitting the virus BTC from individual transport experiments were used as input for fitting the free virus BTC from the co-transport experiments.

tapwater for about two days at the same flow rate. Detailed information on column experiments is given by Walshe et al. (2010).

We assume a one-site linear kinetic model for kaolinite attachment to the gravel. Hence, the developed model with the set of Eqs. (1) and (2) for colloid transport and Eqs. (7), (8), (10) and (12) for virus transport are used to fit the observed breakthrough curves from the co-transport of viruses and colloids under saturated conditions. As a pre-equilibrated solution containing kaolinite and MS2 was applied at the column inlet, it is assumed that equilibrium was reached between the free MS2 and MS2 attached to the colloids in the injection solution. Hence, the following boundary conditions for virus transport are used to model the experimental data of Walshe et al. (2010) for the co-transport experiments (Saiers and Hornberger, 1996) along with Eqs. (16), (21) and (22):

$$c(0,t)=\begin{cases}\dfrac{k_{\mathrm{detmc}}c_0'}{k_{\mathrm{attmc}}+k_{\mathrm{detmc}}} & t\le t_{\mathrm{in}}\\ 0 & t>t_{\mathrm{in}}\end{cases} \tag{31}$$

$$s_{mc}c_{c0}(0,t)=\begin{cases}\dfrac{k_{attmc}c_0'}{k_{attmc}+k_{detmc}} & t\le t_{in}\\ 0 & t>t_{in}\end{cases} \tag{32}$$

where c_0' is the total virus concentration in the injection solution which is the sum of concentrations of free viruses and viruses attached to colloids in the injection solution. Eqs. (15), (17) and (20) describe the initial and boundary conditions for the colloid transport.

The steps followed for fitting the observed BTCs from the co-transport experiments of Walshe et al. (2010) are briefly described here. The pore-water velocity and the dispersivity values were estimated by Walshe et al. (2010), based on the normalized first and second moment of the Bromide BTC. We used those values to calculate the dispersion coefficient of viruses and colloids, given as $D_L{}^c = D_L = \alpha_L v$, where α_L [L] is the dispersivity of the tracer. First, we used our model to fit the virus BTC in the absence of colloids in order to estimate the pore-water velocity of viruses (v) (in case the viruses are observed to travel faster than the tracer), virus attachment (k_{vs}) and detachment (k_{sv}) rate coefficients for the solid surface. Since no BTC of colloids in the absence of viruses was given in Walshe et al. (2010), next we fitted the colloid BTC during the co-transport experiments so as to estimate the pore-water velocity of kaolinite (v_c) (kaolinite was observed to travel faster than the tracer in all experiments) as well as kaolinite attachment and detachment rate coefficients for the solid surface (k_{cs} and k_{sc}). The parameters estimated by fitting the virus BTC from individual transport experiments (v, k_{vs} and k_{sv}) and colloid BTC from the co-transport experiments (v_c, k_{cs} and k_{sc}) were used as input while fitting the free virus BTC from the co-transport experiments. Afterwards, the free virus BTC during the co-transport experiments was fitted so as to estimate the virus attachment and detachment rate coefficients for mobile and immobile colloids (k_{attmc}, k_{attim}, k_{detmc}, k_{detim}), assuming the same rate coefficient for virus interactions with the mobile and immobile colloids ($k_{attmc} = k_{attim}$, $k_{detmc} = k_{detim}$). Knowing all parameter values, we simulated the total mobile virus BTC during the co-transport experiments.

Fig. 5 shows the observed and fitted breakthrough curves for MS2 in the absence of kaolinite, and kaolinite and MS2 breakthrough curves during the co-transport base-case experiment. Fig. 5a, c and d show that in the presence of kaolinite, virus retention significantly increases. This is mainly due to the attachment of MS2 to mobile and immobile kaolinite, which in turn gets retained inside the column. Also both MS2 and kaolinite are found to travel faster than the tracer. The optimized parameter values are given in Table 2. Fig. 5 shows that our model results fit the observed BTCs from individual (Fig. 5a) as well as co-transport (Fig. 5b and c) experiments reasonably well. Also Fig. 5d shows that there is a good agreement between the observed and simulated total mobile virus BTCs.

Fig. 6 together with Fig. 5 show the effect of pH on the co-transport of MS2 and kaolinite. The BTC of MS2 in the absence of kaolinite was given only for the base case (pH = 7.5) in Walshe et al. (2010). Hence for the other experimental conditions, we first fitted the kaolinite BTC during the co-transport experiments so as to estimate the kaolinite transport and deposition parameters (v_c, k_{cs} and k_{sc}). Then, the free MS2 BTC during the co-transport experiments was fitted so as to estimate the four unknown virus deposition parameters, on the grain surface (k_{vs} and k_{sv}) and on colloids ($k_{attmc} = k_{attim}$, $k_{detmc} = k_{detim}$). Finally, we simulated the total mobile virus BTC during the co-transport experiments. The observed and the fitted BTCs for MS2 and kaolinite at pH = 6.5 and pH = 6 during the co-transport experiments are given in Fig. 6. Figs. 5b, 6a, and c show that our model quite well fitted the kaolinite BTCs at all pH values. It must be noted that the fitted values of k_{cs} (dictated by the BTCs) decrease with decreasing pH (Table 2). This is an unexpected trend because a decrease in pH (from 7.5 to 6) shall lead to a decrease in the negative surface charge of kaolinite (as the isoelectric point of kaolinite is reported to be 2.1) (See Chrysikopoulos and Syngouna, 2012). At low negative surface charge, greater will be the retention of kaolinite, and hence larger k_{cs} values are expected. Walshe et al. (2010) do not provide an explanation for this unexpected trend in kaolinite retention with decreasing pH.

In contrast to the observation of decreased colloid retention in the porous medium with decreasing pH, the MS2 retention was observed to increase with decreasing pH. This can be seen from Fig. 5c and d, and Fig. 6b and d which show that both the free and the total mobile MS2 peak concentrations decreased with decreasing pH. Figs. 5c and 6b and d show that there is a good correspondence between the observed free virus BTC (solid circles) and the fitted free virus BTC (solid line) with the virus attachment rate coefficients increasing with decreasing pH (Table 2). This is because as pH decreases, then MS2, gravel and kaolinite become less negatively charged, making the conditions more favorable for MS2 attachment to gravel and kaolinite.

Fig. 7 together with Fig. 5 show the effect of ionic strength on the co-transport of MS2 and kaolinite. They show that as the ionic strength increases, both the colloid and virus effluent concentrations decrease. It can be seen from Fig. 7a and c that there is a good agreement between the observed and the fitted BTCs of kaolinite at different ionic strengths. Also, Fig. 7b and d show that the fitted BTCs of free viruses (solid line) match the observed free virus BTCs (solid circles) during the co-transport experiments at different ionic strengths. Both the colloid and

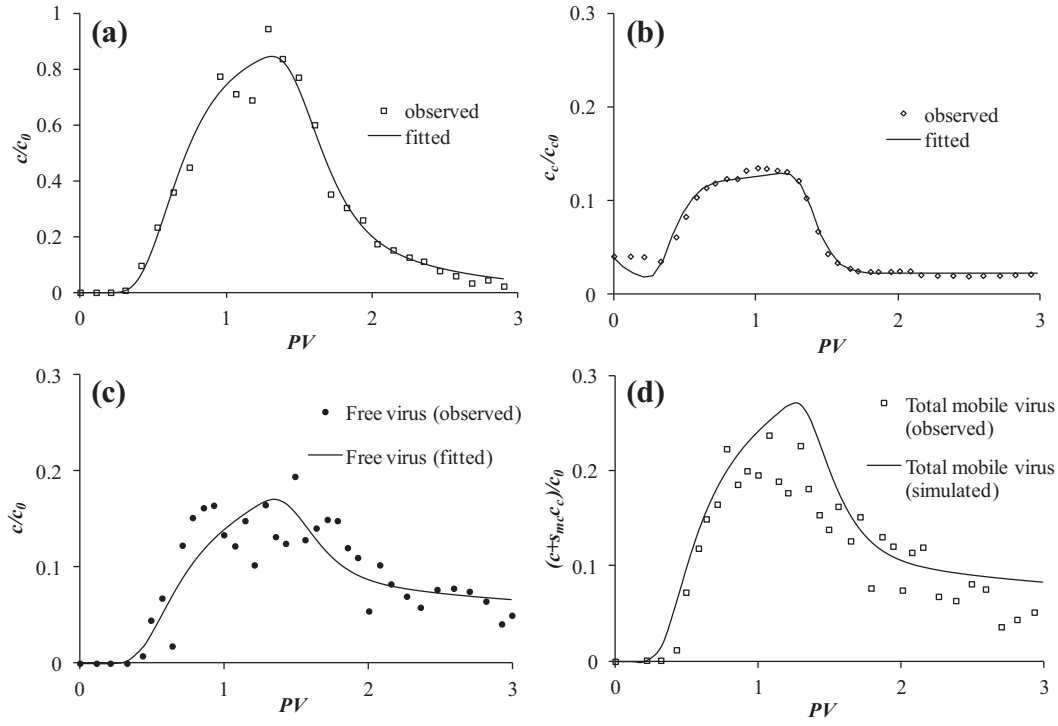

Fig. 5. Observed and fitted breakthrough curves for the base case experiment from Walshe et al. (2010) for (a) MS2 in the absence of kaolinite, (b) kaolinite during the co-transport experiment, (c) free MS2 during the co-transport experiment and (d) total mobile MS2 during the co-transport experiment. (Free virus (fitted): The observed free virus BTC from the experiments is fitted with our model, Total mobile virus (simulated): Total mobile virus BTC is predicted using the parameter values estimated by fitting the free virus BTC).

MS2 rate coefficients of attachment to the solid grains (k_{cs} and k_{vs}) increase with increasing ionic strength (Table 2). This is because as the ionic strength increases, the diffuse double layers around the gravel, kaolinite and MS2 get compressed, making the conditions more favorable for kaolinite and MS2 attachment to the solid grains and also MS2 attachment to kaolinite. Table 2 shows that k_{attmc} decreases with increasing ionic strength, which is not expected. Figs. 6b and 7d show that

Table 2
Fitted values of model parameters for the experimental data of Walshe et al. (2010)[a].

Experiment	Tracer[b]		Colloid[c]				Virus[d]					
pH	v (cm min^{-1})	D_L (cm^2 min^{-1})	v_c (cm min^{-1})	k_{cs} (min^{-1})	k_{sc} (min^{-1})	R^2	v (cm min^{-1})	k_{vs} (min^{-1})	k_{sv} (min^{-1})	k_{attmc} (min^{-1})	k_{detmc} (min^{-1})	R^2(free virus)
7 (base case)	1.417	21.26	2.587 (0.06)	0.0321 (0.0008)	0.00055 (0.00005)	0.98	1.872 (0.09)	0.0033 (0.001)	0.0108 (0.004)	0.0025 (0.0005)	0.0007 (0.0001)	0.76
6.5	1.533	23.0	2.56 (0.05)	0.015 (0.0004)	0.0002 (0.0001)	0.98	1.533	0.0079 (0.02)	0.028 (0.2)	0.0102 (0.03)	0.00197 (0.006)	0.96
6	1.517	21.233	2.702 (0.1)	0.0129 (0.0009)	0.0007 (0.0002)	0.94	1.517	0.143 (0.78)	0.012 (0.09)	0.047 (0.42)	0.0366 (0.47)	0.78
Ionic strength ($cacl_2$)												
0 (base case)	1.417	21.26	2.587 (0.06)	0.0321 (0.0008)	0.00055 (0.00005)	0.98	1.872 (0.09)	0.0033 (0.001)	0.0108 (0.004)	0.0025 (0.0005)	0.0007 (0.0001)	0.76
0.54 mM	1.517	19.717	3.041 (0.26)	0.047 (0.004)	0.00057 (0.0001)	0.79	1.517	0.004 (0.03)	0.001 (0.06)	0.0015 (0.02)	0.0003 (0.003)	0.69
0.72 mM	1.517	24.267	1.915 (0.06)	0.057 (0.002)	0.00029 (0.00003)	0.98	1.517	0.0379 (0.1)	0.004 (0.08)	0.00036 (0.1)	0.0018 (0.5)	0.76

[a] The standard errors associated with the estimated parameter values are given in parentheses.
[b] v and D_L from Walshe et al. (2010).
[c] v_c, k_{cs} *and* k_{sc} obtained by fitting the colloid BTC from co-transport experiments.
[d] For the base case experiment, v, k_{vs} and k_{sv} were obtained by fitting the virus BTC from individual transport experiments. Then, k_{attmc} and k_{detmc} obtained by fitting the free virus BTC from the co-transport experiments assuming $k_{attmc} = k_{attim}$ and $k_{detmc} = k_{detim}$. The values of v_c, k_{cs} *and* k_{sc} obtained by fitting the colloid BTC from co-transport experiments and, v, k_{vs} and k_{sv} obtained by fitting the virus BTC from individual transport experiments were used as input for fitting the free virus BTC from the co-transport experiments. For the other experiments, k_{vs}, k_{sv}, k_{attmc} and k_{detmc} were obtained by fitting the free virus BTC from the co-transport experiments assuming $k_{attmc} = k_{attim}$ and $k_{detmc} = k_{detim}$. The values of v_c, k_{cs} *and* k_{sc} obtained by fitting the colloid BTC from co-transport experiments were used as input for fitting the free virus BTC from the co-transport experiments.

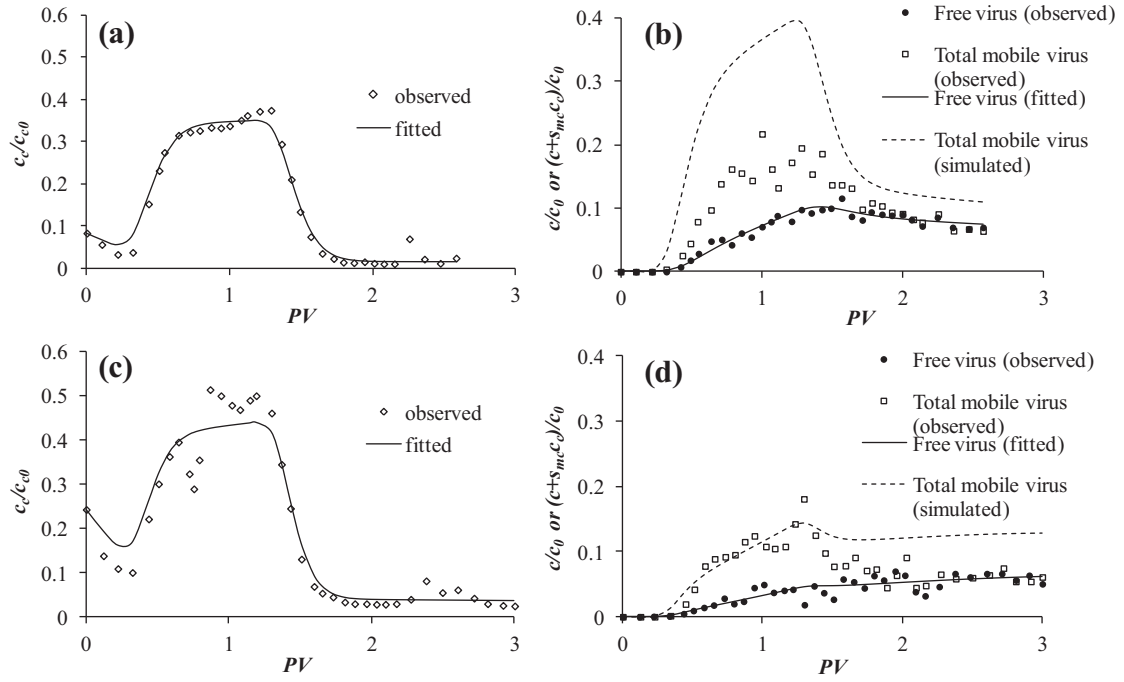

Fig. 6. Observed and fitted BTCs of kaolinite (left column) and MS2 (right column) during co-transport experiments from Walshe et al. (2010) at pH = 6.5 (a and b) and pH = 6 (c and d). (Free virus (fitted): The observed free virus BTC from the experiments is fitted with our model, Total mobile virus (simulated): Total mobile virus BTC is predicted using the parameter values estimated by fitting the free virus BTC).

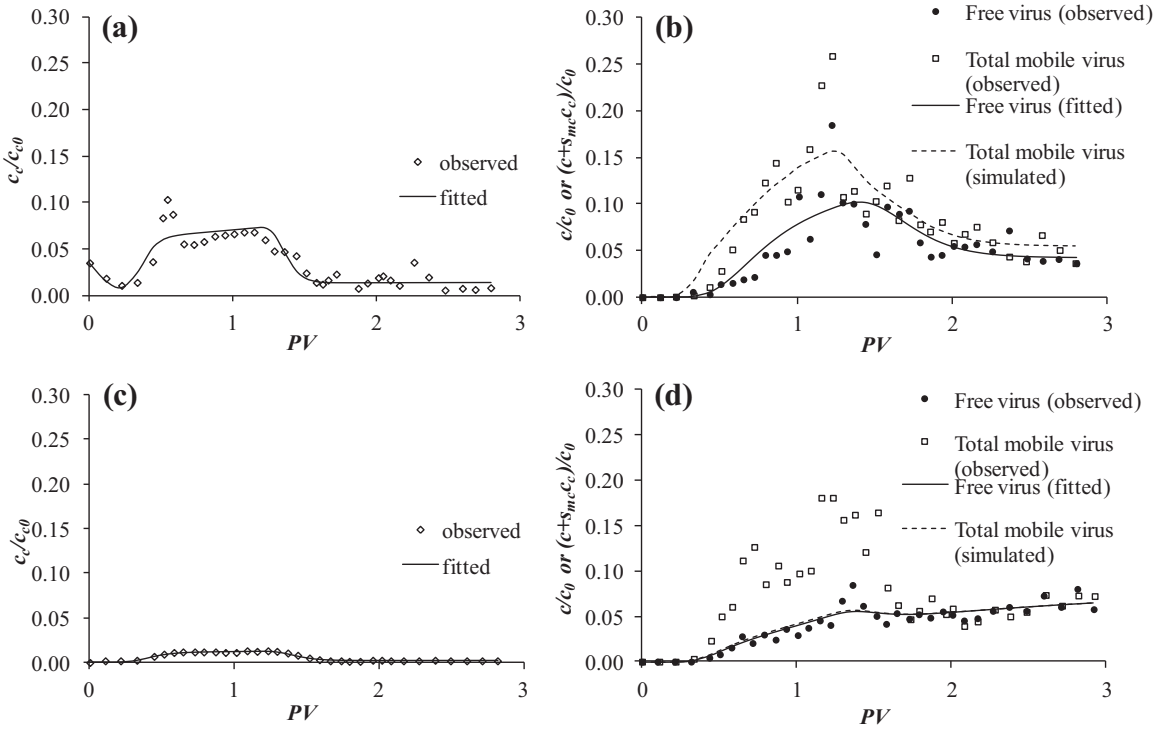

Fig. 7. Observed and fitted BTCs of kaolinite (left column) and MS2 (right column) during co-transport experiments from Walshe et al. (2010) at ionic strength = 0.54 mM $CaCl_2$ (a and b) and ionic strength = 0.72 mM $CaCl_2$ (c and d). (Free virus (fitted): The observed free virus BTC from the experiments is fitted with our model, Total mobile virus (simulated): Total mobile virus BTC is predicted using the parameter values estimated by fitting the free virus BTC).

there is a mismatch between the observed (open squares) and the simulated (dashed lines) total mobile virus BTCs. Based on the personal communications with the authors of Walshe et al. (2010), we know that the gravel used in packing the column had native colloids present on it initially. The amount of resident colloids present on gravel packing is unknown. Also the same column was used for all the experiments. The resident colloid concentration would have certainly been affected by experimental changes of pH and ionic strength. These changes could not be modeled in this study due to the lack of necessary information. Table 2 shows that except for the base case experiment, the standard errors of the estimated parameter values describing virus deposition (k_{vs}, k_{sv}, k_{attmc} and k_{detmc}) during the co-transport experiments are rather large. This could be due to the lack of enough information for the estimation of the four unknown parameters (k_{vs}, k_{sv}, k_{attmc} and k_{detmc}). We also observed that there is a strong correlation among the four estimated parameters.

4.3. Simulation of experiments of Syngouna and Chrysikopoulos (2015)

Syngouna and Chrysikopoulos (2015) studied the effects of clay colloids, kaolinite or montmorillonite, on the transport of bacteriophages, MS2 or ΦX174 in variably saturated porous media. The experiments were conducted in 15.2-cm long columns with 2.6 cm internal diameter, packed with glass beads at two different saturations: (1) fully saturated conditions, and (2) unsaturated conditions (degree of saturation ~ 0.81–0.93). A fresh column was packed for each experiment and the packed column had a porosity of 0.42. A constant flow of 1.5 mL/min in the downward direction was maintained during the experiments. The mean pH of the column influent remained constant at 7.0 ± 0.2 for the duration of each experiment. Two sets of experiments were performed with viruses and clay particles separately, in order to determine their individual transport characteristics. Four sets of co-transport experiments (ΦX174-kaolinite, ΦX174-montmorillonite, MS2-kaolinite and MS2-montmorillonite) were performed to investigate the effect of the presence of clay colloids on virus transport. For each experiment, the clay colloidal suspension and the viral suspension were injected simultaneously into the packed column for three PVs, followed by three PVs of ddH2O. All experiments were carried out at the same flow rate and at room temperature (25 °C). Chloride, in the form of KCl, was chosen as the nonreactive tracer. Detailed information about the experiments is available in Syngouna and Chrysikopoulos (2015).

Deposition of clay colloids onto the solid grains under unsaturated conditions is modeled as a one-site linear kinetic process. Both the colloid and virus attachment to the AWI are best described using a linear irreversible model. Hence, the developed model, with the set of Eqs. (1), (2) and (4) for colloid transport, and Eqs. (7), (8), (9), (10), (12) and (14) for virus transport are used to fit the observed breakthrough curves from the co-transport of colloids and viruses under unsaturated conditions, with the initial and boundary conditions specified by Eqs. (15)–(22). Under saturated conditions, a two-site kinetic model with a reversible and an irreversible site describes colloid deposition onto the SWI. The values of van Genuchten water retention parameters for glass beads used in the fitting are $\alpha = 0.158\ \text{cm}^{-1}$, $n = 6.8$ and $\theta_r = 0.014$ (Kim et al., 2008).

The steps followed for fitting the observed BTCs from the co-transport experiments of Syngouna and Chrysikopoulos (2015) under unsaturated conditions are the same as that described in Section 4.1 for those of Syngouna and Chrysikopoulos (2013). While fitting the virus BTC from individual transport experiments under unsaturated conditions, the virus deposition parameters for the solid surface (k_{vs} & k_{sv}) and AWI (k_{va}) were estimated. Similarly, the colloid deposition parameters for the solid surface (k_{cs} and k_{sc}) and AWI (k_{ca}) were estimated from the colloid BTC of the co-transport experiments. The parameters estimated by fitting the BTC of viruses from the individual transport experiment (k_{vs}, k_{sv} and k_{va}), and colloids from the co-transport experiment (k_{cs}, k_{sc} and k_{ca}) were used as input while fitting the free virus BTC from co-transport experiments under unsaturated conditions. The free virus BTC during the co-transport experiments was fitted so as to estimate the virus attachment and detachment rate coefficients for the mobile and immobile colloids (k_{attmc}, k_{attim}, k_{attima}, k_{detmc}, k_{detim}, k_{detima}), assuming that the rate coefficients of virus interaction with the mobile and immobile colloids are the same ($k_{attmc} = k_{attim} = k_{attima}$, $k_{detmc} = k_{detim} = k_{detima}$). Finally, knowing all parameter values, the total mobile virus BTC during the co-transport experiments under unsaturated experiments was simulated and the results were compared to the experimental data.

Fig. 8 shows the observed and fitted BTCs for colloids and viruses during the co-transport of ΦX174 and montmorillonite under saturated and unsaturated conditions. The model (solid lines) fits the observed BTCs of colloids (open diamonds) and free viruses (open squares) during the co-transport experiments under both saturated (Fig. 8a and b) and unsaturated conditions (Fig. 8c and d) reasonably well. The corresponding values of fitted parameters are given in Table 3. Also, Fig. 8d shows that the simulated (dotted line) and the observed (filled squares) total mobile virus BTCs matches well under unsaturated conditions. Virus retention in porous media during co-transport experiments is greater under unsaturated conditions (Fig. 8d) as compared to the saturated conditions (Fig. 8b). This is due to: (1) increased attachment of viruses and colloids to the SWI, (2) virus attachment to the AWI, and (3) co-deposition of colloids with attached viruses on its surface to the AWI. The fitted values of parameters for the co-transport experiments of MS2-kaolinite and MS2-montmorillonite are also given in Table 3.

5. Simulations for unsaturated conditions and sensitivity analysis

In order to identify the most sensitive parameters affecting virus transport in the presence of colloids under unsaturated conditions, the mathematical model developed in the current study is used to calculate the sensitivity index of various parameters. This is done by performing a sensitivity analysis of the model for 16 parameters, as shown in Table 4. The range of parameter values are taken from the fitting of experimental data of Syngouna and Chrysikopoulos (2013), (2015) and Walshe et al. (2010), presented in previous sections, and also from the literature (Anders and Chrysikopoulos, 2009; Bekhit

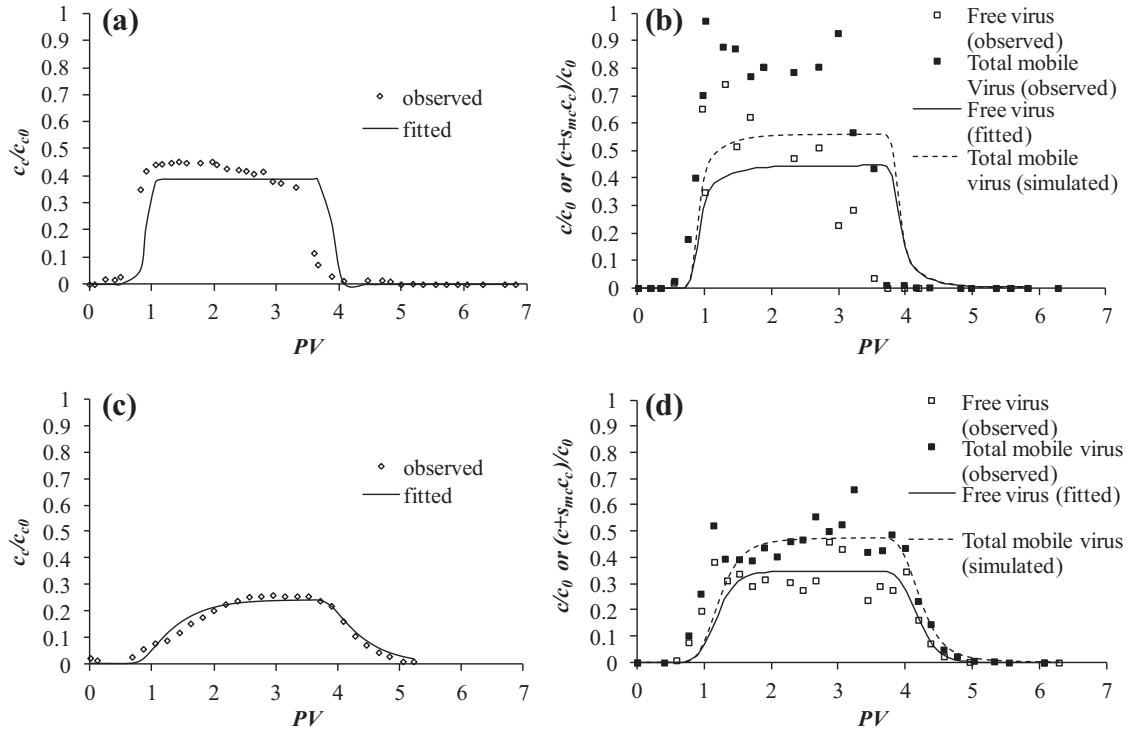

Fig. 8. Observed and fitted BTCs of colloids (left column) and viruses (right column) from Syngouna and Chrysikopoulos (2015) during the co-transport of ΦX174 and montmorillonite at saturated (a and b), and unsaturated (c and d) conditions. (Free virus (fitted): The observed free virus BTC from the experiments is fitted with our model, Total mobile virus (simulated): Total mobile virus BTC is predicted using the parameter values estimated by fitting the free virus BTC).

et al., 2006; Chu et al., 2001; Compere et al., 2001; Corapcioglu and Choi, 1996; Lenhart and Saiers, 2002; Noell et al., 1998; Saiers and Hornberger, 1996; Saiers and Lenhart, 2003; Schafer et al., 1998; Torkzaban et al., 2006a,b; Vasiliadou and Chrysikopoulos, 2011). During the sensitivity analysis, we varied only one of the model parameters, keeping all other parameter values constant. We consider a finite column of sand with uniform saturation and flow. Unless specified, parameter values used in the simulations are the same as those given in Table 5. In the simulations, the colloids and viruses are injected simultaneously and continuously for five PVs followed by flushing the column with a colloid-free and virus-free solution for another five PVs. The virus BTCs are presented in terms of concentrations of free virus (c/c_0) as well as total mobile virus ($(c + s_{mc}c_c)/c_0$).

Fig. 9 shows the BTCs of viruses and colloids from individual transport simulations and co-transport simulations under saturated and unsaturated conditions for the parameter values given in Table 5. Our results prescribe that virus retention in the absence of colloids is greater under unsaturated conditions compared to saturated conditions due to virus attachment to the AWI (Fig. 9a), which is expected. Similarly, the colloid retention is greater under unsaturated conditions compared to saturated conditions due to colloid attachment to the AWI (Fig. 9b). Fig. 9c shows that the virus retention during the co-transport experiments is greater under unsaturated conditions compared to the saturated conditions due to: (1) virus attachment to the AWI and (2) attachment of colloids with attached viruses on its surface to AWI.

The sensitivity analysis of the model to the parameters describing colloid transport revealed that the effluent colloid concentration decreases with increasing k_{cs}, k_{ca} and $s_{ca(\max)}$, and, as a result, the effluent total mobile virus concentration decreases. Also, the difference between the total mobile and the free virus concentration decreases with increasing k_{cs}, k_{ca} and $s_{ca(\max)}$ values. The opposite trend was observed with increasing k_{sc} and c_{c0}.

The sensitivity analysis of the model to the parameters describing virus interactions with the SWI and AWI revealed that both the free and the total mobile virus concentrations decrease with increasing k_{vs} and k_{va} values. Also, the difference between the total mobile and the free virus concentrations decrease with increasing k_{vs} and k_{va} values.

Regarding the parameters describing virus interaction with the mobile and immobile colloids, we find that the free virus concentration decreases and the peak total mobile virus concentration increases with increasing k_{attmc}. Also, the difference between the total mobile virus concentration and the free virus concentration increases with increasing k_{attmc}. An exactly opposite trend was observed with increasing k_{detmc} values. The free virus and the peak total mobile virus concentrations decrease with increasing k_{attim} and k_{attima}, thereby reducing the difference between the total mobile and free virus peak concentrations. The opposite trend was observed with increasing k_{detim} and k_{detima}. Also, as k_{attim} increases, the tail concentration in the free virus BTC decreases once the input pulse is stopped whereas the tail concentration in the total mobile virus BTC increases due to the detachment of

Table 3
Fitted values of model parameters for the experimental data of Syngouna and Chrysikopoulos (2015)[a].

Experiment	Degree of saturation (%)	Individual transport									Co-transport							
		Virus[b]				Colloid[c]					Colloid[d]					Virus[e]		
		k_{vs} (min^{-1})	k_{sv} (min^{-1})	k_{va} (min^{-1})	R^2	k_{cs1} (min^{-1})	k_{sc1} (min^{-1})	k_{cs2} (min^{-1})	k_{ca} (min^{-1})	R^2	k_{cs1} (min^{-1})	k_{sc1} (min^{-1})	k_{cs2} (min^{-1})	k_{ca} (min^{-1})	R^2	k_{attmc} (min^{-1})	k_{detmc} (min^{-1})	R^2 (free virus)
ΦX174-montmorillonite	100	0.018 (0.016)	0.175 (0.19)	–	0.91	0.043 (0.004)	0.17 (0.02)	0.0038 (0.0004)	–	0.99	0.046 (0.003)	~0	~0	–	0.77	0.0133 (0.002)	~0	0.44
	83	0.197 (0.2)	1.05 (1.2)	0.0186 (0.001)	0.91	0.014 (0.003)	0.087 (0.03)	–	0.025 (0.0007)	0.98	0.076 (0.02)	0.197 (0.06)	–	0.069 (0.001)	0.96	0.011 (0.001)	~0	0.73
MS2-kaolinite	100	0.018 (0.04)	0.34 (0.8)	–	0.86	0.23 (0.02)	0.32 (0.03)	0.01 (0.0005)	–	0.99	0.025 (0.01)	0.26 (0.2)	0.058 (0.001)	–	0.9	0.012 (0.001)	~0	0.8
	83	0.016 (0.03)	0.205 (0.5)	0.0125 (0.003)	0.69	0.055 (0.009)	0.161 (0.03)	–	0.036 (0.0008)	0.96	~0	~0	–	0.069 (0.004)	0.62	0.019 (0.002)	0.0014 (0.003)	0.58
MS2-montmorillonite	100	0.018 (0.04)	0.34 (0.8)	–	0.86	0.043 (0.004)	0.17 (0.02)	0.0038 (0.0004)	–	0.99	0.042 (0.001)	~0	~0	–	0.93	0.016 (0.009)	0.00055 (0.001)	0.88
	81	0.016 (0.03)	0.205 (0.5)	0.0125 (0.003)	0.69	0.014 (0.003)	0.087 (0.03)	–	0.025 (0.0007)	0.98	0.0059 (0.003)	0.045 (0.07)	–	0.072 (0.003)	0.93	0.0086 (0.0009)	~ 0	0.85

[a] The standard errors associated with the estimated parameter values are given in parentheses.
[b] Parameters obtained by fitting the virus BTC from individual transport experiments.
[c] Parameters obtained by fitting the colloid BTC from individual transport experiments.
[d] Parameters obtained by fitting the colloid BTC from co-transport experiments.
[e] k_{attmc} and k_{detmc} obtained by fitting the free virus BTC from the co-transport experiments assuming $k_{attmc} = k_{attim} = k_{attima}$ and $k_{detmc} = k_{detim} = k_{detima}$. The values of colloid deposition parameters obtained by fitting the colloid BTC from co-transport experiments and virus deposition parameters obtained by fitting the virus BTC from individual transport experiments were used as input for fitting the free virus BTC from the co-transport experiments.

Table 4
Range of parameter values for the sensitivity analysis.

Parameter	Range
k_{cs} (min^{-1})	5×10^{-4}–0.1
k_{sc} (min^{-1})	5×10^{-5}–0.5
k_{ca} (min^{-1})	0.001–0.1
k_{vs} (min^{-1})	10^{-5}–0.01
k_{sv} (min^{-1})	10^{-6}–0.1
k_{va} (min^{-1})	5×10^{-5}–0.1
k_{attmc}, k_{attim}, k_{attima} (min^{-1})	5×10^{-4}–0.05
k_{detmc}, k_{detim}, k_{detima} (min^{-1})	10^{-4}–0.1
$s_{ca\ (max)}$ (mg/cm^2 AWI)	10^{-8}–0.001
$s_{a\ (max)}$ (pfu/cm^2 AWI)	10^4–10^6
C_{c0} (mg/mL)	10–100
C_{v0} (pfu/mL)	10^5–10^{10}

colloids from SWI, which had more virus attached on it. As k_{attima} increases, the tail concentration in free virus BTC decreases once the input pulse is stopped. As the colloids are irreversibly attached to the AWI, the tail concentration in the total mobile virus BTC decreases with increasing k_{attima}.

In order to quantitatively describe the effect of various parameters on the virus transport in the presence of colloids, we have calculated the sensitivity index for each parameter as follows (Hamby, 1994):

$$\text{Sensitivity Index, } SI = \frac{c_{\max} - c_{\min}}{c_{\max}}$$

where $c_{\max}$ and $c_{\min}$ are the maximum and the minimum effluent concentration values when varying the parameter over its entire range. Sensitivity index represents the percentage change in the output when varying one parameter from its minimum to the maximum value. In order to study the effect of various parameters on different parts of the BTC, we calculated the *SI* at five different pore volumes: 1 (rising limb), 2 & 5 (plateau), 6 (declining limb), and 10 (tail). Fig. 10 shows the sensitivity index of various parameters at those five pore volumes. It can be seen from Fig. 10 that the rate coefficient for attachment of viruses to the AWI, k_{va}, is the most sensitive parameter affecting the free and total mobile virus BTCs for the range of parameter values considered in this study and it has a significant effect on all parts of the BTC. The free and the total mobile virus BTCs are mainly influenced by parameters describing virus attachment to the AWI (k_{va}), virus interactions with mobile and immobile colloids (k_{attmc}, k_{attim}, k_{attima}, k_{detmc}, k_{detim}, k_{detima}), virus attachment to SWI (k_{vs}), and colloid interaction with SWI and AWI (k_{cs}, k_{sc}, k_{ca}). The virus BTC is relatively insensitive to $s_{ca(\max)}$, c_{c0}, k_{sv}, $s_{a(\max)}$ and c_{v0}. The colloid deposition parameters have a significant effect only on the tail portion of the free virus BTC, whereas they become less significant in the tail portion of the total mobile virus BTC.

Table 5
Model parameters used in the simulation.

Parameter	Value
Column length, *L* (cm)	30
Column diameter (cm)	2.5
Saturated water content, θ_s	0.375
Residual moisture content, θ_r	0.053
α (cm^{-1})	0.0352
n	3.17687
Degree of saturation (%)	60
Water content, θ	0.225
Flow rate, *Q* (mL min^{-1})	0.5
Darcy velocity, *q* (cm min^{-1})	0.1
Pore-water velocity, *v* (cm min^{-1})	0.45
Dispersivity, λ (cm)	0.4
C_{c0} (mg/mL)	10
C_{v0} (pfu/mL)	10^6
k_{cs} (min^{-1})	0.005
k_{sc} (min^{-1})	5×10^{-4}
k_{ca} (min^{-1})	0.01
k_{vs} (min^{-1})	10^{-4}
k_{sv} (min^{-1})	10^{-5}
k_{va} (min^{-1})	0.001
k_{attmc}, k_{attim}, k_{attima} (min^{-1})	0.01
k_{detmc}, k_{detim}, k_{detima} (min^{-1})	5×10^{-4}
$s_{ca\ (max)}$ (mg/cm^2 AWI)	10^{-4}
$s_{a\ (max)}$ (pfu/cm^2 AWI)	10^5

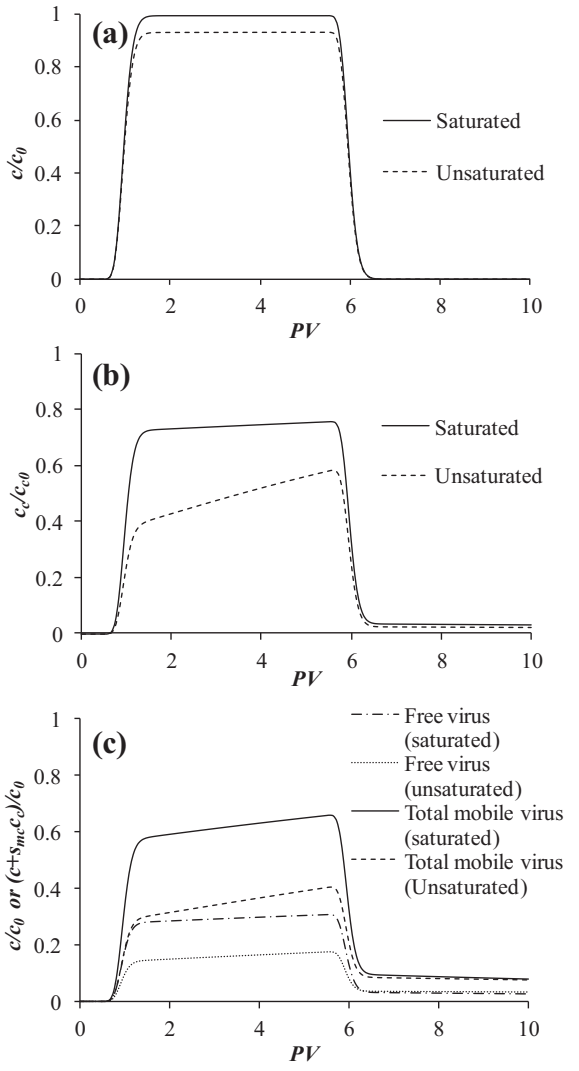

Fig. 9. BTCs of (a) viruses during individual transport, (b) colloids during co-transport and, (c) free and total mobile viruses during co-transport simulations at saturated and unsaturated conditions.

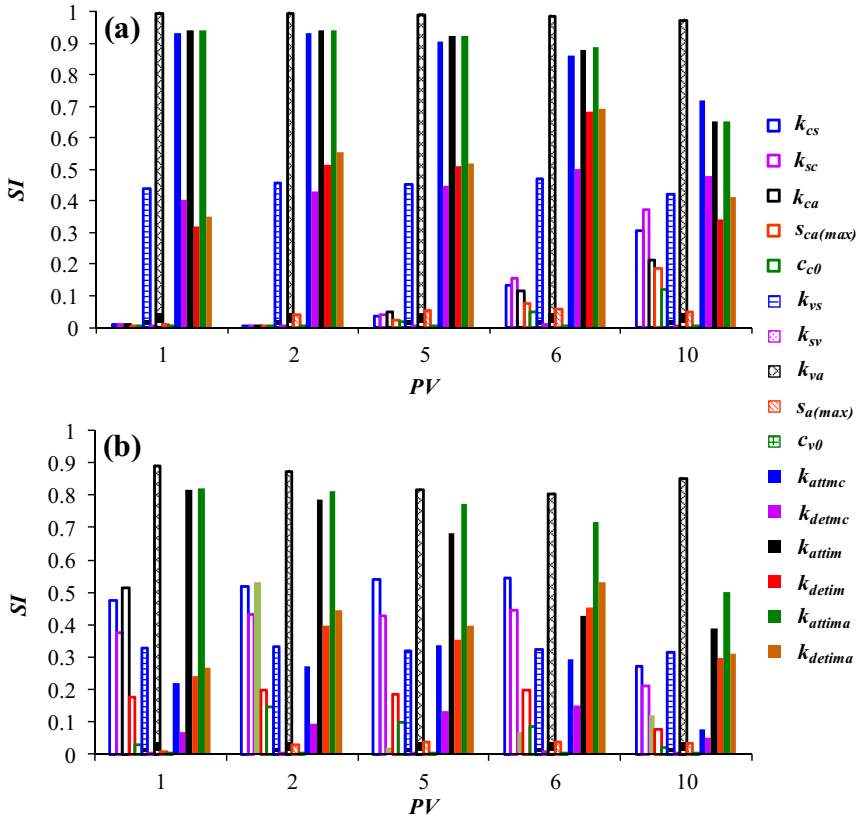

Fig. 10. Sensitivity index of various parameters describing virus and colloid transport at different pore volumes for (a) free viruses and (b) total mobile viruses.

6. Conclusions

We have developed a mathematical model to simulate the co-transport of viruses and colloids in unsaturated porous media under steady-state flow conditions. The governing equations are solved numerically using an alternating three-step operator splitting approach. The model is verified by fitting the experimental data of (1) Syngouna and Chrysikopoulos (2013) and (2) Walshe et al. (2010), who studied the co-transport of viruses and clay colloids under saturated conditions, and (3) Syngouna and Chrysikopoulos (2015) for the co-transport of viruses and clay colloids under unsaturated conditions. The model results are found to be in good agreement with the observed BTCs under both saturated and unsaturated conditions. Following this, the developed model was used to simulate the co-transport of viruses and colloids in porous media under unsaturated conditions. The virus retention in the presence of colloids is greater during unsaturated conditions as compared to the saturated conditions due to: (1) virus attachment to the AWI, and (2) co-deposition of colloids with attached viruses on its surface to AWI. A sensitivity analysis of the model to various parameters showed that the virus attachment to the AWI is the most sensitive parameter affecting both the free and the total mobile virus BTCs for the range of parameter values considered in this study and has a significant effect on all parts of the BTC. The free and the total mobile virus BTCs are mainly influenced by parameters describing virus attachment to the AWI, virus interactions with mobile and immobile colloids, virus attachment to SWI, and colloid interaction with SWI and AWI. The virus BTC is relatively insensitive to parameters describing the maximum adsorption capacity of the AWI for colloids, inlet colloid concentration, virus detachment rate coefficient from the SWI, maximum adsorption capacity of the AWI for viruses and inlet virus concentration.

Nomenclature

A_{AWI}	Specific area of the AWI [$L^2\ L^{-3}$]
$B(w, z)$	Beta function of w and z [–]
c	Free virus concentration in the aqueous phase [pfu L^{-3}]
c_0	Inlet free virus concentration [pfu L^{-3}]
c_0'	Total virus concentration in the injection solution [pfu L^{-3}]
c_c	Mass concentration of colloids in the aqueous phase [ML^{-3}]
c_{c0}	Inlet colloid concentration [ML^{-3}]
D_L	Dispersion coefficient of viruses [L^2T^{-1}]
D_L^c	Dispersion coefficient of colloids [L^2T^{-1}]
g	Gravitational constant [LT^{-2}]
$I_u(w, z)$	Incomplete beta function of w and z
k_{attim}	Virus attachment rate coefficient for the immobile colloids at SWI [T^{-1}]
k_{attima}	Virus attachment rate coefficient for the immobile colloids at AWI [T^{-1}]
k_{attmc}	Virus attachment rate coefficient for the mobile colloids [T^{-1}]

k_{ca}	Colloid attachment rate coefficient for AWI [T^{-1}]
k_{cs}	Colloid attachment rate coefficient for SWI [T^{-1}]
k_{detim}	Virus detachment rate coefficient from the immobile colloids at SWI [T^{-1}]
k_{detima}	Virus detachment rate coefficient from the immobile colloids at AWI [T^{-1}]
k_{detmc}	Virus detachment rate coefficient from the mobile colloids [T^{-1}]
k_{sc}	Colloid detachment rate coefficient from SWI [T^{-1}]
k_{sv}	Virus detachment rate coefficient from SWI [T^{-1}]
k_{va}	Virus attachment rate coefficient for AWI [T^{-1}]
k_{vs}	Virus attachment rate coefficient for SWI [T^{-1}]
L	Length of the column [L]
m	van Genuchten water retention function parameter [–]
n	van Genuchten water retention function parameter [–]
q	Darcy flux [LT^{-1}]
q_c	Darcy flux of colloids [LT^{-1}]
s	Virus concentration adsorbed to SWI [pfu M^{-1}]
s_a	Virus concentration adsorbed to AWI [pfu L^{-2}]
$s_{a(\max)}$	Maximum adsorption capacity of AWI for viruses [pfu L^{-2}]
s_c	Colloid mass fraction adsorbed to SWI [MM^{-1}]
s_{ca}	Colloid concentration adsorbed to AWI [ML^{-2}]
$s_{ca(\max)}$	Maximum adsorption capacity of AWI for colloids [ML^{-2}]
SI	Sensitivity Index [–]
s_{im}	Virus concentration attached to immobile colloids at SWI [pfu M^{-1}]
s_{ima}	Virus concentration attached to immobile colloids at AWI [pfu M^{-1}]
s_{mc}	Virus concentration attached to mobile colloids [pfu M^{-1}]
t	Time [T]
t_{in}	Duration of the input pulse [T]
v	Pore-water velocity [LT^{-1}]
v_c	Pore-water velocity of colloids [LT^{-1}]
z	Spatial coordinate [L]
α	van Genuchten water retention function parameter [L^{-1}]
ψ_c	Langmuir blocking function for colloid attachment to the AWI [–]
ψ_v	Langmuir blocking function for virus attachment to AWI [–]
ρ	Density of water [ML^{-3}]
ρ_b	Bulk density of the porous medium [ML^{-3}]
σ	Surface tension of water [MT^{-2}]
θ	Water content [–]
θ_r	Residual water content [–]
θ_s	Saturated water content [–]
Θ	Relative saturation [–]

Acknowledgements

The first author thanks Prof. Jack F. Schijven (National Institute for Public Health and the Environment, The Netherlands), and Prof. Markus Flury (Washington State University, USA) for the very useful discussions, and Dr. Liping Pang (Institute of Environmental Science and Research, New Zealand) for the email communications. She also acknowledges a grant from Utrecht University (grant no. WA.146130.4) for a three-month visit to The Netherlands.

References

Anders, R., Chrysikopoulos, C.V., 2009. Transport of viruses through saturated and unsaturated columns packed with sand. Transp. Porous Media 76, 121–138.

Bales, R.C., Hinkle, S.R., Kroeger, T.W., Stocking, K., 1991. Bacteriophage adsorption during transport through porous media: chemical perturbations and reversibility. Environ. Sci. Technol. 25, 2088–2095.

Barry, D.A., Bajracharya, K., Crapper, M., Prommer, H., Cunningham, C.J., 2000. Comparison of split-operator methods for solving coupled chemical non-equilibrium reaction/groundwater transport models. Math. Comput. Simul. 53, 113–127.

Bekhit, H.M., Hassan, A.E., Harris-Burr, R., Papelis, C., 2006. Experimental and numerical investigations of effects of silica colloids on transport of strontium in saturated sand columns. Environ. Sci. Technol. 40, 5402–5408.

Bekhit, H.M., El-Kordy, M.A., Hassan, A.E., 2009. Contaminant transport in groundwater in the presence of colloids and bacteria: Model development and verification. J. Contam. Hydrol. 108, 152–167.

Cai, L., Tong, M., Wan, X., Kim, H., 2014. Influence of clay particles on the transport and retention of titanium dioxide nanoparticles in quartz sand. Environ. Sci. Technol. 48, 7323–7332.

Cary, J.W., 1994. Estimating the surface area of fluid phase interfaces in porous media. J. Contam. Hydrol. 15, 243–248.

Chen, G., Flury, M., Harsh, J.B., 2005. Colloid-facilitated transport of cesium in variably saturated Hanford sediments. Environ. Sci. Technol. 39, 3435–3442.

Choi, H., Corapcioglu, M.Y., 1997. Transport of a non-volatile contaminant in unsaturated porous media in the presence of colloids. J. Contam. Hydrol. 25, 299–324.

Chrysikopoulos, C.V., Syngouna, V.I., 2012. Attachment of bacteriophages MS2 and ΦX174 onto kaolinite and montmorillonite: extended-DLVO interactions. Colloids Surf. B: Biointerfaces 92, 74–83.

Chu, Y., Jin, Y., Flury, M., Yates, M.V., 2001. Mechanisms of virus removal during transport in unsaturated porous media. Water Resour. Res. 37 (2), 253–263.

Compere, F., Porel, G., Delay, F., 2001. Transport and retention of clay particles in saturated porous media: influence of ionic strength and pore velocity. J. Contam. Hydrol. 49, 1–21.

Corapcioglu, M.Y., Choi, H., 1996. Modeling colloid transport in unsaturated porous media and validation with laboratory column data. Water Resour. Res. 32 (12), 3437–3449.

Corapcioglu, M.Y., Jiang, S., 1993. Colloid-facilitated groundwater contaminant transport. Water Resour. Res. 29 (7), 2215–2226.

Corapcioglu, M.Y., Kim, S., 1995. Modeling facilitated contaminant transport by mobile bacteria. Water Resour. Res. 31 (11), 2639–2647.

de Jonge, H., Jacobsen, O.H., de Jonge, L.W., Moldrup, P., 1998. Colloid-facilitated transport of pesticide in undisturbed soil columns. Phys. Chem. Earth 23 (2), 187–191.

Flury, M., Qiu, H., 2008. Modeling colloid-facilitated contaminant transport in the vadose zone. Vadose Zone J. 7 (2), 682–697.

Gasda, S.E., Farthing, M.W., Kees, C.E., Millet, C.T., 2011. Adaptive split-operator methods for modelling transport phenomena in porous medium systems. Adv. Water Resour. 34, 1268–1282.

Grolimund, D., Borkovec, M., Barmettler, K., Sticher, H., 1996. Colloid-facilitated transport of strongly sorbing contaminants in natural porous media: a laboratory column study. Environ. Sci. Technol. 30, 3118–3123.

Hamby, D.M., 1994. A review of techniques for parameter sensitivity analysis of environmental models. Environ. Monit. Assess. 32, 135–154.

Hijnen, W.A.M., Brouwer-Hanzens, A.J., Charles, K.J., Medema, G.J., 2005. Transport of MS2 phage, *Escherichia coli*, *Clostridium perfringens*, *Chryptosporidium parvum*, and *Giardia intestinalis* in a gravel and a sandy soil. Environ. Sci. Technol. 39, 7860–7868.

Jiang, S., Corapcioglu, M.Y., 1993. A hybrid equilibrium model of solute transport in porous media in the presence of colloids. Colloids Surf. A Physicochem. Eng. Asp. 73, 275–286.

Jin, Y., Pratt, E., Yates, M., 2000. Effect of mineral colloids on virus transport through saturated sand columns. J. Environ. Qual. 29, 532–540.

Kaluaracbchi, J.J., Morshed, J., 1995. Critical assessment of the operator-splitting technique in solving the advection–dispersion–reaction equation: 1. First-order reaction. Adv. Water Resour. 18 (2), 89–100.

Kanti Sen, T., Shanbhag, S., Khilar, K.C., 2004. Subsurface colloids in groundwater contamination: a mathematical model. Colloids Surf. A Physicochem. Eng. Asp. 232, 29–38.

Katzourakis, V.E., Chrysikopoulos, C.V., 2014. Mathematical modeling of colloid and virus cotransport in porous media: application to experimental data. Adv. Water Resour. 68, 62–73.
Keller, A.A., Sirivithayapakorn, S., Chrysikopoulos, C.V., 2004. Early breakthrough of colloids and bacteriophage MS2 in a water-saturated sand column. Water Resour. Res. 40, W08304.
Kim, S., Corapcioglu, M.Y., 1996. A kinetic approach to modeling mobile bacteria-facilitated groundwater contaminant transport. Water Resour. Res. 32 (2), 321–331.
Kim, S., Corapcioglu, M.Y., 2002a. Contaminant transport in dual-porosity media with dissolved organic matter and bacteria present as mobile colloids. J. Contam. Hydrol. 59, 267–289.
Kim, S., Corapcioglu, M.Y., 2002b. Contaminant transport in riverbank filtration in the presence of dissolved organic matter and bacteria: a kinetic approach. J. Hydrol. 266, 269–283.
Kim, S., Corapcioglu, M.Y., Kim, D., 2003. Effect of dissolved organic matter and bacteria on contaminant transport in riverbank filtration. J. Contam. Hydrol. 66, 1–23.
Kim, M., Kim, S., Park, S., 2008. Bacteria transport in an unsaturated porous media: incorporation of air–water interface area model into transport modeling. Hydrol. Process. 22, 2370–2376.
Knappett, P.S.K., Emelko, M.B., Zhuang, J., McKay, L.D., 2008. Transport and retention of a bacteriophage and microspheres in saturated, angular porous media: effects of ionic strength and grain size. Water Res. 42, 4368–4378.
Lenhart, J.J., Saiers, J.E., 2002. Transport of silica colloids through unsaturated porous media: experimental results and model comparisons. Environ. Sci. Technol. 36, 769–777.
Loveland, J.P., Ryan, J.N., Amy, G.L., Harvey, R.W., 1996. The reversibility of virus attachment to mineral surfaces. Colloids Surf. A Physicochem. Eng. Asp. 107, 205–221.
Massoudieh, A., Ginn, T.R., 2007. Modeling colloid-facilitated transport of multi-species contaminants in unsaturated porous media. J. Contam. Hydrol. 92, 162–183.
Niemet, M.R., Rockhold, M.L., Weisbrod, N., Selker, J.S., 2002. Relationship between gas–liquid interfacial surface area, liquid saturation, and light transmission in variably saturated porous media. Water Resour. Res. 38 (8), 1135.
Noell, A.L., Thompson, J.L., Corapcioglu, M.Y., Triay, I.R., 1998. The role of silica colloids on facilitated cesium transport through glass bead columns and modeling. J. Contam. Hydrol. 31, 23–56.
Pang, L., Simunek, J., 2006. Evaluation of bacteria-facilitated cadmium transport in gravel columns using the HYDRUS colloid-facilitated solute transport model. Water Resour. Res. 42. http://dx.doi.org/10.1029/2006WR004896.
Pang, L., Close, M.E., Noonan, M.J., Flintoft, M.J., van den Brink, P., 2005. A laboratory study of bacteria-facilitated cadmium transport in alluvial gravel aquifer media. J. Environ. Qual. 34, 237–247.
Putti, M., Yeh, W.W.G., Mulder, W.A., 1990. A triangular finite volume approach with high-resolution upwind terms for the solution of groundwater transport equations. Water Resour. Res. 26 (12), 2865–2880.
Ratha, D.N., Hari Prasad, K.S., Ojha, C.S.P., 2009. Analysis of virus transport in groundwater and identification of transport parameters. Pract. Period. Hazard. Toxic Radioact. Waste Manage. 13 (2), 98–109.
Roy, S.B., Dzombak, D.A., 1997. Chemical factors influencing colloid-facilitated transport of contaminants in porous media. Environ. Sci. Technol. 31, 656–664.
Sadeghi, G., Schijven, J.F., Behrends, T., Hassanizadeh, S.M., Gerritse, J., Kleingeld, P.J., 2011. Systematic study of effects of pH and ionic strength on attachment of phage PRD1. Ground Water 49 (1), 12–19.
Sadeghi, G., Behrends, T., Schijven, J.F., Hassanizadeh, S.M., 2013. Effect of dissolved calcium on the removal of bacteriophage PRD1 during soil passage: the role of double-layer interactions. J. Contam. Hydrol. 144, 78–87.
Saiers, J.E., Hornberger, G.M., 1996. The role of colloidal kaolinite in the transport of cesium through laboratory sand columns. Water Resour. Res. 32 (1), 33–41.
Saiers, J.E., Lenhart, J.J., 2003. Ionic-strength effects on colloid transport and interfacial reactions in partially saturated porous media. Water Resour. Res. 39 (9), 1256.
Schafer, A., Ustohal, P., Harms, H., Stauffer, F., Dracos, T., Zehnder, A.J.B., 1998. Transport of bacteria in unsaturated porous media. J. Contam. Hydrol. 33, 149–169.
Schijven, J.F., Hassanizadeh, S.M., 2000. Removal of viruses by soil passage: overview of modeling, processes, and parameters. Crit. Rev. Environ. Sci. Technol. 30 (1), 49–127.
Simunek, J., Sejna, M., van Genuchten, M.Th., 2012. The C-Ride Module for HYDRUS (2D/3D) Simulating two-dimensional colloid-facilitated solute transport in variably-saturated porous media. Version 1.0. PC Progress, Prague, Czech Republic.
Simunek, J., He, C., Pang, L., Bradford, S.A., 2006. Colloid-facilitated transport in variably-saturated porous media: numerical model and experimental verification. Vadose Zone J. 5, 1035–1047.
Sirivithayapakorn, S., Keller, A., 2003. Transport of colloids in unsaturated porous media: a pore-scale observation of processes during the dissolution of air–water interface. Water Resour. Res. 39 (12), 1346.
Soraganvi, V.S., Mohan Kumar, M.S., 2009. Modeling of flow and advection dominant solute transport in variably saturated porous media. J. Hydrol. Eng. 14 (1), 1–14.
Syngouna, V.I., Chrysikopoulos, C.V., 2012. Transport of biocolloids in water saturated columns packed with sand: effect of grain size and pore water velocity. J. Contam. Hydrol. 129–130, 11–24.
Syngouna, V.I., Chrysikopoulos, C.V., 2013. Cotransport of clay colloids and viruses in water saturated porous media. Colloids Surf. A Physicochem. Eng. Asp. 416, 56–65.
Syngouna, V.I., Chrysikopoulos, C.V., 2015. Experimental investigation of virus and clay particles in partially saturated columns packed with glass beads. J. Colloid Interface Sci. 440, 140–150.
Torkzaban, S., Hassanizadeh, S.M., Schijven, J.F., de Bruin, H.A.M., de Roda Husman, A.M., 2006a. Virus transport in saturated and unsaturated sand columns. Vadose Zone J. 5, 877–885.
Torkzaban, S., Hassanizadeh, S.M., Schijven, J.F., van den Berg, H.H.J.L., 2006b. Role of air–water interfaces on retention of viruses under unsaturated conditions. Water Resour. Res. 42, W12S14.
van de Weerd, H., Leijnse, A., 1997. Assessment of the effect of kinetics on colloid facilitated radionuclide transport in porous media. J. Contam. Hydrol. 26, 245–256.
Vasiliadou, I.A., Chrysikopoulos, C.V., 2011. Cotransport of *Pseudomonas putida* and kaolinite particles through water-saturated columns packed with glass beads. Water Resour. Res. 47, W02543.
Walshe, G.E., Pang, L., Flury, M., Close, M.E., Flintoft, M., 2010. Effects of pH, ionic strength, dissolved organic matter, and flow rate on the co-transport of MS2 bacteriophages with kaolinite in gravel aquifer media. Water Res. 44, 1255–1269.
Wan, J., Wilson, J.L., 1994a. Colloid transport in unsaturated porous media. Water Resour. Res. 30 (4), 857–864.
Wan, J., Wilson, J.L., 1994b. Visualization of the role of the gas–water interface on the fate and transport of colloids in porous media. Water Resour. Res. 30 (1), 11–23.
Yan, Y.D., 1996. Pulse-injection chromatographic determination of the deposition and release rate constants of colloidal particles in porous media. Langmuir 12, 3383–3388.
Yang, H., Tong, M., Kim, H., 2012. Influence of bentonite particles on representative gram negative and gram positive bacterial deposition in porous media. Environ. Sci. Technol. 46, 11627–11634.
Yates, M.V., Gerba, C.P., Kelley, L.M., 1985. Virus persistence in groundwater. Appl. Environ. Microbiol. 49 (4), 778–781.
Zhang, Q., Karadimitriou, N.K., Hassanizadeh, S.M., Kleingeld, P.J., Imhof, A., 2013a. Study of colloids transport during two-phase flow using a novel polydimethylsiloxane micro-model. J. Colloid Interface Sci. 401, 141–147.
Zhang, Q., Hassanizadeh, S.M., Karadimitriou, N.K., Raoof, A., Liu, B., Kleingeld, P.J., Imhof, A., 2013b. Retention and remobilization of colloids during steady-state and transient two-phase flow. Water Resour. Res. 49, 8005–8016.
Zhuang, J., Jin, Y., 2002. Virus retention and transport as influenced by different forms of soil organic matter. J. Environ. Qual. 32, 816–823.
Zhuang, J., Jin, Y., 2008. Interactions between viruses and goethite during saturated flow: effects of solution pH, carbonate and phosphate. J. Contam. Hydrol. 98, 15–21.